

May 24, 1999

# Simulated (Un)binding of Arachidonic Acid in the Cyclooxygenase Site of Prostaglandin H<sub>2</sub> Synthase-1

Ferenc Molnar\*, Lawrence S. Norris#, and Klaus Schulten\*,§

\*Beckman Institute, University of Illinois at Urbana-Champaign, 405

North Mathews, Urbana, Illinois 61801, and #Departments of

Biomedical Engineering and Chemistry, Northwestern University,

2145 Sheridan, Evanston, IL 60208

phone: 217-244-2212

fax: 217-244-6078

**Running Title:** Simulated (Un)binding in PGHS-1

**Keywords:** steered molecular dynamics, targeted molecular dynamics, forced unbinding, forced binding, pathways, enzyme–substrate binding

---

§ To whom correspondence should be addressed (email: *kschulte@ks.uiuc.edu*). Animations of our trajectories can be obtained at the web-site <http://www.ks.uiuc.edu/Research/pghs/>

## Abstract

Molecular Dynamics simulations with external forces are employed to study the unbinding and binding of Arachidonic Acid (AA) in the cyclooxygenase (COX) site of Prostaglandin H<sub>2</sub> Synthase-1. Simulations with AA inside the COX binding channel reveal sequences of concerted bond rotations in the fatty acid alkyl chain which obviate the need for gross conformational changes in the protein and substrate during unbinding and binding. The all-*cis* structure of AA, with double bonds separated by two single bonds, facilitates easy access to the COX channel and correct positioning inside the active site for the COX chemistry to occur. Two derivatives of AA, one with a *cis* double bond changed to a *trans* configuration and the other with a double bond reduced to a single bond, are also studied. In both cases the concertedness of bond rotations in the fatty acid chain is diminished and larger forces are required to move the fatty acid inside the COX channel. Important motions of residues near the mouth of the COX channel are found and analyzed. In particular, a conformational “switch“ involving Arg83, Glu524 and Arg120 is seen to mediate the movement of the substrate from the membrane to the channel.

Prostaglandin H<sub>2</sub> synthase (PGHS) is a membrane-associated protein that catalyzes the first committed step in the conversion of arachidonic acid (AA), a 20 carbon tetraenoic fatty acid (all-*cis* 5,8,11,14-eicosatetraenoic acid), to various prostaglandins (Otto and Smith, 1995; Smith and DeWitt, 1995; Smith and DeWitt, 1996; Smith *et al.*, 1996). The overall product of the enzymatic reaction is PGH<sub>2</sub> which is formed in PGHS autocatalytically from PGG<sub>2</sub> in a two step reaction AA → PGG<sub>2</sub> → PGH<sub>2</sub>. There are many prostaglandins (also known as prostanoids) and the precursor to them all is PGH<sub>2</sub>. The metabolic cascade from AA to prostanoids is known as the *arachidonic cascade*. Prostaglandins play a role in almost every physiological system and in many pathophysiological states. Moreover the enzyme is the site of action of the non-steroidal anti-inflammatory drugs (NSAIDS) such as Aspirin, Tylenol, Ibuprofen and Naproxen Sodium (Alleve). Therefore, there is much interest in revealing in detail the mechanism of this enzyme (Smith and DeWitt, 1995; Smith and DeWitt, 1996; Masferrer *et al.*, 1996; Herschman, 1996; Kalgutkar *et al.*, 1998; Callan *et al.*, 1996; Swinney *et al.*, 1997; So *et al.*, 1998).

There exist two identified isoforms of PGHS, PGHS-1 and PGHS-2. The two enzymes are nearly completely homologous in their primary structures and, hence, in their higher level structures as well. PGHS-1 is constitutively expressed and acts in normal “housekeeping” functions of homeostasis. PGHS-2 is only expressed upon induction by some pathophysiological signal. Most currently available NSAIDS are active against both PGHS-1 and PGHS-2, but inhibition of PGHS-1 leads to a derangement of normal prostaglandin mediated homeostasis. This inhibition further results in side effects such as gastric bleeding, renal failure, and platelet disaggregation. Therefore, finding drugs that inhibit PGHS-2 but not PGHS-1 is a major research goal. Significant differences in the two isoforms between

the geometries of their fatty acid binding channels can be exploited by drug designers. This paper focuses on the influence of the structure of the binding channel in PGHS-1 on the binding of AA.

The first PGHS molecule crystallized was the ovine-1 isoform (Picot *et al.*, 1994). This protein, presented in Fig. 1, is composed of two identical subunits related by a non-crystallographic two-fold symmetry axis. Each monomeric subunit has 576 residues with molecular mass of nearly 70 kDa and is constituted of three structural domains. The first domain, comprised of residues 34-72, is similar to the epidermal growth factor (EGF) and establishes contacts between the two monomeric units. The second domain (residues 73-116) is involved in membrane binding and contains for this purpose mostly hydrophobic residues arranged in a spiral of four right handed helices; these helices anchor the monomer to one leaflet of the membrane bilayer. The third domain is responsible for the enzymatic function. PGHS is actually bifunctional, possessing both peroxidase (POD) and cyclooxygenase (COX) activity.

*Figure 1*

The POD and COX active sites are distinct and spatially separated. The POD active site, which is structurally homologous to other known plant, fungal and animal peroxidases, is near the top (in Fig. 1) of the protein and is exposed to the solvent so that peroxides and exogenous substrates have easy access to it. The COX site on the other hand is situated deep in the interior of the enzyme and is accessible only through a long hydrophobic channel, 12 Å long and 6 Å wide. The fatty acid substrate (AA) enters the channel at the bottom of the protein from the lipid bilayer. In the channel the substrate assumes a bent conformation such that the *pro-S* hydrogen at C-13 is properly positioned to be abstracted by an activated tyrosine (Tyr385). It is important to note that PGG<sub>2</sub> is made in the COX active site and

*here*

that it exits the channel back into the leaflet of the lipid bilayer to which PGHS is anchored. From there PGG<sub>2</sub> is partitioned out to the aqueous phase without traversing the membrane and is able to reach the POD active site to be finally reduced to PGH<sub>2</sub>. The available experimental data on structure (Picot *et al.*, 1994; Luong *et al.*, 1996; Kurumbail *et al.*, 1996) as well as on reaction and inhibition kinetics (Swinney *et al.*, 1997; Callan *et al.*, 1996; So *et al.*, 1998) of PGHS give only limited insight into the access mechanism of substrate and inhibitors to the COX site. Indeed structural changes which account, e.g., for the time-dependent inhibition of COX by NSAIDS, do not involve large scale static conformational changes (Kurumbail *et al.*, 1996).

The questions which need to be pursued in order to understand the access mechanism are: What is the nature of the conformational changes associated with the binding of AA occurring in the protein and in the fatty acid itself? How is the selectivity of PGHS towards AA determined? What are the key amino acid residues and their specific function in binding AA? These questions are addressed in this paper.

The following residues line the COX channel presented in Fig. 1: Val116, Leu117, Ile345, Tyr348, Val349, Leu352, Leu359, Leu384, Trp387, Phe518, Met522, Ile523, Gly526, Ala527, Ser530, Leu531, and Leu534; Tyr385 is at the end of the channel and Arg120, Ser353, Tyr355, Glu524 are at the mouth of the channel (see Fig. 1). Experimental observations reveal a role of the latter residues in substrate binding and configurational selectivity (Luong *et al.*, 1996; Kurumbail *et al.*, 1996; So *et al.*, 1998). The monotopic arrangement of the enzyme in the membrane allows the substrate to leave the lipid phase directly into the hydrophobic COX channel (Picot and Garavito, 1994). Most likely, the carboxylate group of the fatty acid is picked out of the bilayer by electrostatic interaction with Arg120 or

Arg83, which are located at the protein/membrane interface. Conformational shifts of the residues near the channel opening, as well as in the fatty acid itself, along with fluctuations in residues that line the channel, facilitate motion of AA from the membrane to the COX site.

The conformational changes in the substrate required for entering or leaving the binding pocket are not amenable to standard molecular dynamics (MD) simulations since these events take place on a millisecond to second time scale (So *et al.*, 1998; Callan *et al.*, 1996; Swinney *et al.*, 1997; Luong *et al.*, 1996). Simulations with external forces (Leech *et al.*, 1996; Grubmüller *et al.*, 1996; Izrailev *et al.*, 1997; Balsera *et al.*, 1997; Isralewitz *et al.*, 1997; Lüdemann *et al.*, 1997; Stepaniants *et al.*, 1997; Marrink *et al.*, 1998; Lu *et al.*, 1998; Hermans *et al.*, 1998; Izrailev *et al.*, 1998; Kosztin *et al.*, 1999; Schlitter *et al.*, 1993; Ma and Karplus, 1997; Wu and Wang, 1998), however, allow one to bridge the gap between the picosecond to nanosecond time scale of MD simulations and the time scale of the actual biochemical reactions by introducing external forces which accelerate binding and unbinding. In this paper Steered Molecular Dynamics (SMD) and Targeted Molecular Dynamics (TMD) simulations of the unbinding/binding of AA from/to the COX binding site of PGHS-1 are presented. The results explain the selectivity of PGHS-1 for AA compared to similar fatty acids (Smith and DeWitt, 1995), identify residues essential for the selection of AA and suggest a probable binding mechanism for AA to the COX active site of PGHS-1.

The next section describes the methods used to simulate and analyze the unbinding/binding of AA. The Results and Discussion section presents force profiles and other observables which characterize the structure-dynamics relationship of unbinding/binding of

AA. The Conclusion section summarizes the suggested mechanism for substrate selectivity and binding.

## Methods

### Simulations

Simulations were carried out *in vacuo* for one monomeric subunit of PGHS-1 with AA bound in its putative COX site. The exclusion of the second subunit (see Fig. 1) implies, that the dynamics of the substrate in the binding pocket is independent of the state of the other monomeric unit of the homo-dimer. From the crystal structure it appears that each monomer is chemically independent in as much as activation of one monomer does not necessary affect the other. This assumption does not contradict experimental observations, but is also not directly supported by observation. However, there exists an observation that suggests that the protein can loose its structural integrity, hence its function, if Cys69 is mutated to Ser69, which leads to an unraveling of the EGF domain and a subsequent separation of the monomers (Otto and Smith, 1995). Indeed, in order to achieve a stable monomer structure *in vacuo*, it was necessary in our simulations to constrain at least the C $_{\alpha}$  atoms of the interface region and the membrane binding motif (Val33 up to Leu117) to their positions in the energy minimized structure with a force constant of 350 pN/Å, all other atoms were allowed to move freely in our simulations.

In all simulations the CHARMM22 force field (Brooks *et al.*, 1983; MacKerell Jr. *et al.*, 1995) and the SMD method as implemented in the parallel molecular dynamics program NAMD (Nelson *et al.*, 1996) were used. The length of the timestep was 1 fs and configurations were stored every 100 timesteps. TMD calculations were carried out with a serial version of the NAMD code. ChelpG charges for AA adopting its conformation in the binding site were obtained with Gaussian94 (Frisch *et al.*, 1995) at the HF/6-31G\* level.

The coordinates for PGHS-1 were taken from the entry 1pth of the Protein Data Bank (Bernstein *et al.*, 1977) with hydrogens added using the HBUILD procedure of X-PLOR (Brünger, 1992). AA was assumed to be deprotonated carrying a charge of -1.

The initial placement of AA in the COX channel corresponds to a model structure (Garavito *et al.*, personal communication). A crystal structure with AA bound in the COX site is not available. Modeling of alternative conformations of AA in the COX channel was attempted but no other energetically acceptable conformations of the substrate in the narrow channel than the one obtained here were found. An important constraint on the conformation of AA in the active site is that the transformation of AA to PGG<sub>2</sub> begins with the abstraction of the pro-S hydrogen of C13 by an activated Tyr385 radical (Schreiber *et al.*, 1986; Tsai *et al.*, 1995). The distance between the oxygen atom of Tyr385 and the C13 carbon is 3.3 Å in our model structure. The distance between the pro-S hydrogen and the oxygen atom is 2.7 Å. These distances are well within range for a powerful oxidant such as a Tyr radical to be reduced by what is effectively a pentadiene, a powerful reducing agent (Tsai *et al.*, 1998).

No membrane lipids were included in the model. The structure was minimized at 0K and then heated within 50 ps to 300K in order to remove unfavorable contacts. After this relaxation phase, the system was equilibrated for additional 50 ps prior to the SMD and TMD simulations. A cutoff of 14 Å, with a switching function starting at 12 Å, was applied to long-range interactions.

## SMD

In SMD simulations an external force is applied to permit a system to overcome barriers in a shorter time than in conventional MD simulations (Grubmüller *et al.*, 1996; Izrailev *et al.*, 1997; Balseira *et al.*, 1997; Isralewitz *et al.*, 1997; Stepaniants *et al.*, 1997; Lu *et al.*, 1998; Izrailev *et al.*, 1998; Kosztin *et al.*, 1999). In the current study the external force was applied to AA through a harmonic spring with slowly moving endpoint according to the equation

$$\vec{F} = k(\vec{x}_0 + \vec{v}t - \vec{x}). \quad (1)$$

Here  $k$  is the stiffness of the spring,  $v = |\vec{v}|$  is the velocity of the endpoint, and  $\vec{x}_0$  is the initial position of the endpoint. In the present study the spring was attached to the carbon of the methyl-end group of the fatty-acid chain (C20), shown in Fig. 2 and Fig. 3, with position  $\vec{x}$  at time  $t$ . C20 is pulled along a direction, defined by  $\vec{v}$ , pointing out of the binding pocket through an opening in the protein surface as depicted in Fig. 4a,b. The pulling direction was identified by visual inspection of the equilibrated structure using VMD (Humphrey *et al.*, 1996). The external force and the velocity should be chosen so that the system achieves sufficient conformational sampling and that the barriers along the unbinding pathway are not overcome too rapidly. In the initial phase of SMD simulations with “soft springs” (small  $k$  values), the influence of the external force on the ligand is small and an almost linear increase in  $F(t)$  is observed, modulated only by the thermal fluctuations of the ligand in its binding pocket. The slope of this initial increase is proportional to  $kv$ . As soon as the external force is large enough to overcome the barriers hindering motion of AA, the ligand starts to move in the pulling direction, and the distance to the restraint point decreases.

According to Eq. 1 this will result in a drop in the external force. After such an event, the movement of the ligand might be hindered again by a new potential barrier and the external force will start to increase again. The resulting structure of the force profile, the shape and height of the observed peaks, is one of the main sources of information in the analysis of the SMD trajectories. SMD simulations in our study enforce unbinding rather than binding of the ligand, but the data collected in the simulation nevertheless provide useful information about the binding pathway.

*Figure 2*

*here*  
*Figure 3*

## TMD

The TMD method is usually applied to induce large conformational changes in biopolymers on the time scale of MD simulations (Schlitter *et al.*, 1993; Ma and Karplus, 1997). An initial and a desired target structure of the system define a suitable pathway between the two states. TMD imposes time-dependent holonomic constraints  $\Phi$  leading to a constraining force  $\vec{F}^c$  which drives the system from one known state to another (Schlitter *et al.*, 1993).  $\Phi$  and  $\vec{F}^c$  are defined through

*here*  
*Figure 4*

*here*

$$\Phi(\vec{r}) = (\vec{r} - \vec{r}_T)^2 - \rho^2 = 0, \quad \vec{F}^c = \lambda \vec{\nabla} \Phi(\vec{r}). \quad (2)$$

The prescribed distance between the current geometry given by coordinates  $\vec{r}$  and the target structure  $\vec{r}_T$  is denoted by  $\rho$ . The distance  $\rho$  is slowly decreased to zero during the course of the TMD simulation.  $\lambda$  is an adjustable Lagrange parameter. This strategy can also be employed to study the unbinding/binding of ligands from/to the active sites of proteins, if both the bound and unbound structures are given. The original TMD method (Schlitter

*et al.*, 1993) applies constraints to all  $N$  atoms in a given system, i.e.,  $\vec{r} \in \mathbb{R}^{3N}$ . However, for the problem at hand it is sufficient to introduce external forces acting only on the  $n$  atoms of the ligand ( $n = 53$ ), i.e.,  $\vec{r} \in \mathbb{R}^{3n}$ . If the constraints are applied to a single atom only ( $n = 1$ ), one arrives at a method similar in spirit to SMD, but with a different underlying time dependent potential.

The TMD method requires specification of the time allowed to reach the final state from the initial state. For the present study the time specified was 100 ps resulting in forces smaller than 200 pN on individual atoms of AA. The effect of an extended time scale was investigated by allowing 40 ns for the unbinding. Since the constraining force depends linearly on the distance from the target geometry (cf., Eq. 2), and the positions of protein atoms in the initial and target structures are very similar, the strongest constraining forces will act on the substrate in the beginning of the trajectory, and the protein atoms will remain relatively unimpacted by the constraining force.

In the TMD simulations of ligand unbinding, the initial state structures were identical to those used in the SMD simulations; for the TMD target structures, PGHS-1 was equilibrated without the substrate in the channel and AA was placed near the entrance of the channel in an extended conformation in a position which would correspond to a location inside the membrane. The TMD simulations of ligand binding were carried out with the initial and target states interchanged.

## **Analysis**

In order to investigate the details of the relationship between the structure and dynamics of the COX channel to those of the substrate fatty acid, alterations were introduced into

the structure of AA for some of the SMD and TMD simulations. All-*cis* AA was changed into its 8-*trans* isomer (AA<sub>t</sub>), and alternatively into an AA derivative for which the double bond C8=C9 is a single bond (AA<sub>s</sub>). The resulting structures are shown in Figs. 2 and 3. Comparison of the AA, AA<sub>t</sub>, and AA<sub>s</sub> trajectories allowed us to expose the importance of certain substrate motions that facilitate binding. For the calculation of energies, force profiles, and time-series of internal coordinates the procedures implemented in X-PLOR were applied to trajectories calculated by NAMD.

Concerted large amplitude motions of the residues forming the binding pocket and of AA were analyzed by the “essential dynamics” (ED) method (van Aalten *et al.*, 1996). The ED method involves the construction of a covariance matrix  $\mathbf{C}$  with elements:

$$C_{ij} = \langle (r_i - r_{i,0})(r_j - r_{j,0}) \rangle, \quad (3)$$

where the  $r_i$  are Cartesian coordinates of  $N$  atoms ( $i = 1, \dots, 3N$ ).  $\mathbf{C}$  is diagonalized and the eigenvectors associated with the largest eigenvalues of  $\mathbf{C}$  indicate the important concerted motions of atoms in the system. Calculation of matrix elements requires the specification of reference positions  $r_{i,0}$  for atoms. Usually the reference positions for a system in equilibrium are set equal to the time average of atomic positions calculated over the whole trajectory. SMD and TMD simulations, however, involve transitions between different states of the system which include, for example, translational motions of the ligand. The drift in the system conformation induced by the SMD and TMD methods requires one to define  $r_{i,0}$  as follows: for those parts of the enzyme-substrate system for which no significant structural changes are observed the  $r_{i,0}$  are defined through the averaged structure; for the part of the

system involved in significant motions the initial state defines the  $r_{i,0}$ 's.

## Results and Discussion

In this section we present first the force and displacement profiles obtained from SMD simulations of the unbinding process of each of the three fatty acids. Next an analysis of bond angles and ED is employed to demonstrate that during the time course of unbinding the motions of AA are highly localized around a series of neighboring bonds and that there are no extended motions of the protein that facilitate the exit of fatty acids from the channel. We also discuss the behavior of residues near the mouth of the channel during AA unbinding and consider the effect of water molecules at the channel opening. Finally TMD simulations are presented which confirm the SMD results of AA unbinding.

### SMD simulations

#### Force and displacement profiles

Force and displacement profiles, as discussed in Section Methods, constitute the main information that can be extracted from SMD simulations. The unbinding of AA from PGHS was studied under a variety of conditions and using different protocols for the SMD simulations. The resulting trajectories depend on the conditions chosen for  $v$ ,  $k$ , and the pulling direction (Izrailev *et al.*, 1997; Balsera *et al.*, 1997; Kosztin *et al.*, 1999). Results of calculations with  $v = 0.1 \text{ \AA/ps}$  and  $k = 42 \text{ pN/\AA}$  are representative of all SMD simulations performed in the present studies.

Force profiles resulting from simulations of unbinding, of AA, AA<sub>t</sub>, and AA<sub>s</sub> are shown in Fig. 5. In the case of AA, unbinding occurs in clearly resolved stages, while the unbinding of AA<sub>t</sub> and AA<sub>s</sub> is less structured and requires higher forces. The force profiles display small

fluctuations relative to their total magnitude which is due to the relatively small value of  $k$  that was chosen. Comparing the force profiles to displacements in the position of C20 in the bottom panels of Fig. 5 reveals that each force drop is associated with a major movement of the fatty acid tail. Different steps of the unbinding process can clearly be identified, and the movement of the tail is less abrupt for AA (four stages) than for AA<sub>t</sub> (three stages) and AA<sub>s</sub> (two stages). For AA the unbinding involves the steps presented in Table 1 (cf., Fig. 5a,d).

*Figure 5*

The AA<sub>t</sub> force and position profiles shown in Fig. 5b,e have a structure different from that found for AA (cf., Table 2). The first 40 ps of AA<sub>t</sub> unbinding reveal a reorientation of the fatty acid tail towards the entrance of the binding channel in the case of AA<sub>t</sub> but not of AA (cf., Fig. 5b,e *vs.* Fig. 5a,d), where the tail is already oriented favorably initially for an exit from the binding pocket (cf., Figs. 2, 4). The same reorientation is also observed during the first 40 ps of the SMD simulation of AA<sub>s</sub>. The remaining segment of the AA<sub>s</sub> trajectory, shown in Fig. 5c and Fig. 5f, is qualitatively different from that of both AA and AA<sub>t</sub> (cf., Table 3).

*here*  
*Table 1*

*here*

*Table 2*

Shifting the force trace of AA in Fig. 5a by 40 ps one matches the critical segment of the force trace of AA<sub>t</sub> in Fig. 5b. The initial slope of both traces is the same, as it should be because it only depends on  $v$  and  $k$  which are the same in both simulations. Similarly, the position graphs in Fig. 5d,e can be overlaid by 40 ps and 4 Å shifts. The stages of unbinding for AA<sub>t</sub> have been numbered according to the stages observed for AA. The results indicate that not all the stages observed in the AA case are also seen in the AA<sub>t</sub> case. The first force maximum for AA measures 500 pN, whereas it measures 650 pN for AA<sub>t</sub>, and 550 pN for AA<sub>s</sub>. The difference arises from torsions near the modified C8=C9

*here*  
*Table 3*

*here*

bond. In  $AA_t$  and  $AA_s$  the torsions necessary for the unbinding step associated with the force maxima are more hindered than for AA.

These torsional motions involve bonds near  $C5=C6$  and  $C8=C9$  in AA as seen in Fig. 6. As shown in Fig. 6a the transitions  $(1) \rightarrow (2) \rightarrow (3)$  for AA involve mainly concerted rotations near the the  $C8=C9$  bond, while the transitions  $(3) \rightarrow (4) \rightarrow (5)$ , depicted in Fig. 6d, involve concerted rotations near  $C5=C6$ . This sequence of torsional motions is presented in Fig. 7. Transition  $(5) \rightarrow (6)$  of AA involves mainly rotations around the single bonds between C4 and AA's carboxylate head (not shown). The main steps of AA's unbinding are,  $(1) \rightarrow (3)$  and  $(3) \rightarrow (5)$ , which involve consecutive concerted rotations near the  $C8=C9$  and  $C5=C6$  bonds (see also Fig. 5d). From Fig. 6a it can be concluded, that the dihedral angle motions become uncorrelated as soon as the  $C8=C9$  double bond leaves the binding channel at 220 ps (cf., Fig. 7). Nothing comparable is seen for the  $C8=C9$  bond of  $AA_t$  and the  $C8-C9$  bond of  $AA_s$ . The replacement of a *cis*  $C8=C9$  bond (AA) by a *trans*  $C8=C9$  bond ( $AA_t$ ) and by a single  $C8-C9$  bond ( $AA_s$ ) disrupts the correlation of concerted counter-rotations seen for AA in Fig. 7 around 200 ps. In  $AA_t$  no major torsional events are observed before the force reaches 650 pN at 200 ps (Fig. 5b). At this point the force becomes large enough to allow the fatty acid chain to “jump” [ $(2) \rightarrow (5)$ ] over (3) as shown in Fig. 5e, the initial torsional event in the case of AA, by means of a simultaneous torsion near the  $C8=C9$  and  $C5=C6$  bonds (cf., Fig. 6b,e). Under the influence of the external force  $AA_s$  exits the COX channel partially in a major torsional event at 240 ps. The other stages in the displacement profile, i.e., (2) and (3) of Fig. 5f, do not correlate with torsional events as shown in Fig. 6c,f.

The main energetic barrier that the tail of AA needs to overcome in order to complete

*Figure 6*

*here*  
*Figure 7*

*here*

its exit from the COX channel is the non-bonding interaction with the residues forming the “doorway” to the binding site: Arg120, Ile523, Tyr355, Met113, and, especially, Val116 and Leu359 presented in Fig. 4. After the initial reorientation of the tail region of AA<sub>t</sub> and AA<sub>s</sub> discussed above, AA<sub>t</sub> and AA<sub>s</sub> are in an equally favorable orientation as AA to exit the binding pocket. The main unbinding event occurs, however, much later for AA<sub>t</sub> [(2)→(4)] and for AA<sub>s</sub> [(2)→(3)] than for AA [(2)→(3)], at approximately 200 ps as opposed to 140 ps (Figs. 5 and 6). This is reflected also in an increased force necessary for the primary step of unbinding, which involves torsional motions of the fatty acid chain near the altered bond (c.f, Fig. 7). The main contribution for energetically unfavorable interactions comes from the non-bonding energy of the hydrogen atoms of the fatty acid near the C8-C9 bond, which come into close contact with surrounding residues (data not shown).

### **Correlated motions revealed through ED**

An ED analysis was carried out for the unbinding process of AA. Figure 8 shows the results of this analysis averaged over the full length of an SMD trajectory. Only residues lining the binding pocket and the exit pathway of AA were included in the analysis. The eigenvectors with the five largest amplitudes of the respective correlation matrix reveal the main motions involved in the unbinding. The hydrophobic residues lining the binding channel display mainly rotations of their methyl end-groups, but do not exhibit pronounced side-chain reorientation. The largest side-chain reorientation near the COX site is observed for Met522. The strong variation in the position of Arg83 indicates a large amplitude motion of this residue which is discussed further below. Arg120 and Tyr355 experience only moderate variations in their positions indicating that AA can exit the COX site without

causing much disturbance in this region.

*Figure 8*

The flexible fatty acid chain of AA has many torsional degrees of freedom leading to complicated patterns of motion which are difficult to analyze. In order to verify the results of the previous section, the ED methodology was also applied to analyze the nature of concerted motions in AA. Only the eigenvector with the largest eigenvalue was considered for this analysis presented in Table 4. Figures 9 and 10 show the results of this analysis for the main transformations observed during the SMD simulation. The picture that emerges from these results is in accord with the analysis of the SMD simulations reconfirming that the motions involved in the transitions are indeed correlated and localized to certain regions in AA.

*here*

In summary, it was determined that in order to unbind AA from the COX channel by pulling at its methyl end (C20), the “kink” in the fatty acid chain has to traverse the carbon chain from its original position around C10 (cf., Fig. 2) towards the carboxylate head at C1. The SMD trajectory shows that this process involves a sequence of torsions around bonds which becomes hindered, when the kink reaches the C8=C9 double bond. Instead of the torsionally rigid double bonds, the neighboring single bonds undergo concerted rotations. As a result large amplitude motions of the chain as a whole in the narrow hydrophobic channel are avoided. This scenario is disrupted when the *cis* C8=C9 bond is altered (AA → AA<sub>t</sub>, AA<sub>s</sub>).

*Table 4*

*here*

*Figure 9*

*here*

*Figure 10*

*here*

### **Conformational changes in PGHS-1**

The discussion up to this point was mainly concerned with the conformational changes occurring in the substrate. In the following sections conformational changes occurring in and

near the PGHS-1 COX channel are presented. Key residues are identified and their specific role in the (un)binding process is discussed.

**Hydrogen bonding network** The hydrogen bonding network located at the entrance of the COX binding channel consists of Arg120, Tyr355, and Glu524 (So *et al.*, 1998; Luong *et al.*, 1996; Kurumbail *et al.*, 1996). When PGHS-2 binds the inhibitor RS-57067, Arg513 induces a “switch” between this network denoted as N(Arg120/Glu524/-Tyr355) and a different arrangement of hydrogen bonds denoted as N(Arg513/Glu524/-Tyr355) (So *et al.*, 1998). In the latter case Arg513 binds Glu524 which in turn releases Arg120 into a more flexible state. Swinney *et al.* (So *et al.*, 1998) suggest that the enzyme is *relaxed* for N(Arg513/Glu524/Tyr355) and in its activated form whereas in case of N(Arg120/Glu524/Tyr355) the enzyme is *tightened* and in its unactivated form. However, in PGHS-1 Arg513 is replaced by His513. According to Swinney *et al.* the interaction between His513 and Glu524 might not be strong enough to switch the state of the enzyme between the activated and unactivated form.

From the SMD simulations emerges a candidate for inducing this switch, namely Arg83. This side group is able to adopt two different conformations, one bound to residues Thr80, Pro84, Gly471, and one bound to Glu524; the latter conformation enables larger motions of Arg120 as shown in Fig. 11. After binding to Arg83, Glu524 severs the hydrogen bonds to Arg120 and the root mean square deviation of Arg120 with respect to its average position in the equilibrated structure increases from 0.5 Å to 1.0 Å. In the suggested state Arg120 still keeps its hydrogen bond to Tyr355, i.e., the original hydrogen bonding network of PGHS-1, i.e., N(Arg120/Glu524/Tyr355), is reduced to hydrogen bond pairs N(Arg83/Glu524) and

N(Arg120/Tyr355) as presented in Fig. 11.

*Figure 11*

*here*

**Influence of water** PGHS is inserted into one half of a lipid bilayer. Since the phospholipid-heads at the interface between the globular part of the enzyme and the membrane are surrounded by water molecules (Wiener and White, 1992; Heller *et al.*, 1993), the latter are likely to be present near the entrance of the COX channel. The localized effect of such water molecules was examined by placing ten water molecules near this area and minimizing as well as equilibrating the resulting system. The water molecules influence the hydrogen bonding network at the entrance of the binding channel establishing hydrogen bonds to residues Arg83, His90, Arg120, Tyr355, Ser471, Glu524, and to the carboxylate group of AA as shown in Fig. 12 while weakening interactions between the residues of the original network. This weakening is reflected in the SMD force profile presented in Fig. 13. The presence of water molecules widens the entrance to the binding site and AA is extracted more readily. The ensuing sequence of unbinding events given in Table 5 is very similar to that arising during unbinding of AA without water molecules (cf., Table 1 and Fig. 5a,d).

*Figure 12*

Another important function of Arg83, besides its ability to switch the hydrogen bonding network, becomes evident when the SMD trajectories are followed beyond the complete exit of AA from its binding channel [(1)  $\rightarrow$  (5)]. After AA has exited the binding channel, it is pulled further, and the force increases again. Several novel distinct features arise in the force profiles (Fig. 13, (6)  $\rightarrow$  (9)). The first transition after exiting, i.e. (6)  $\rightarrow$  (7), is due to a rotation of the side-chain of Arg120 shown in Fig. 12 which opens the binding pocket completely. Arg120 swings away from Tyr355 and the original hydrogen bonding network is destroyed. In this configuration the guanidinium group of Arg83 helps to bind the

*here*

*Figure 13*

*here*

*Table 5*

*here*

carboxylate head of the fatty acid. When the SMD simulation is continued further, Arg83 takes over binding of AA [(7)  $\rightarrow$  (8)] and Arg120 returns to its original orientation which closes the binding pocket such that N(Arg120,Tyr355,Glu524) is restored. This scenario is observed in the presence of water molecules as well as in simulations without water molecules present at the entrance to the COX site.

The simulations further reveal that after these events AA can be detached from PGHS-1 with a maximum observed force of  $F = 950$  pN [(8)  $\rightarrow$  (9)]. The presence of water molecules aided this unbinding through screening the salt-bridge between Arg83 and AA. Six water molecules remained associated with the reestablished hydrogen bonding network at the entrance to the COX site, while two water molecules followed the carboxylate head of AA after the complete detachment from Arg83. Two further water molecules remained associated with Arg83 and became part of the main hydrogen bonding network of the other six water molecules as Arg83 returned to its equilibrium position. None of the water molecules entered the hydrophobic binding channel during the course of the simulation.

## **TMD simulations**

TMD simulations can model unbinding as well as binding of AA in the COX channel. The results of TMD unbinding simulations can be directly compared to corresponding SMD runs. The binding simulations assume a model in which the membrane was omitted from the simulations and thus the influence of surrounding lipids on AA is not accounted for. No major differences were observed between the TMD simulations with constraints on all the atoms of the enzyme-substrate system and simulations with constraining forces acting only on AA. Therefore, only results for simulations with constraints acting on all atoms are

presented below.

### Unbinding of AA and AA<sub>t</sub>

Figure 14a, shows the total constraining forces acting on all of AA's and AA<sub>t</sub>'s atoms to induce unbinding. Due to the strong fluctuations in the constraining force, an analysis similar to the SMD force profiles is not feasible but the plots of the C20 position carry information which is useful for a comparison with the SMD results. One can recognize that in the TMD simulations much larger external forces were required for unbinding than in the SMD simulations. The unbinding of AA<sub>t</sub> requires yet larger forces than the unbinding of AA which is consistent with the respective SMD simulations.

*Figure 14*

Figure 14c presents the distance of C20 from its initial position. One cannot discuss marked stages in the unbinding process as in the case of the SMD simulations (Fig. 5). This is not surprising, since in the TMD simulations the constraining forces act on all the substrate atoms which induces a translational motion steering the ligand out of the binding pocket, with AA remaining partially folded into the “U-shape” that it has adopted initially. Superimposed on this lateral translation is an “unraveling” of the fatty acid chain depicted in the top part of Fig. 14, which agrees with the unraveling observed in the SMD simulations. The translational component of the motion results in a “smoother” unbinding in the TMD simulations compared to the SMD results but it requires stronger forces. For the ligand to exit the binding pocket in a partially folded “U-shape”, the opening in the doorway to the binding channel has to be larger than in the SMD simulations, where the dominating contribution to unbinding is the movement of the fatty acid tail (compare Figs. 7 and 14). The product of the COX reaction PGG<sub>2</sub> will probably exit the binding pocket by a similar

*here*

translational motion, because its structure contains a five-ring which prevents unraveling motions as in AA.

In our TMD simulations AA exited the binding pocket within 100 ps even though the prescribed time for completing the transition from initial to target structure (see Methods) had been set to 40 ns.

### **Binding of AA**

The binding trajectories show a behavior of AA, depicted in Fig. 14b,d, which is different from a simple inversion of the unbinding trajectory. Due to the absence of interactions with lipids of the bilayer and due to the U-shaped target structure of the TMD simulations AA adopts a U-shape, as seen in Fig. 15, already outside the binding pocket. Out of this configuration the methyl-end of the alkyl chain entered the binding pocket first. The hydrophobic environment of the binding channel and the constraining forces lead to a further movement of the tail into the binding pocket which was stopped at the apex of the channel near Tyr385. The simulations continued until the alkyl chain bent itself towards the exit and reached a configuration very similar to the target configuration. The occurrence of such a “U-shaped” AA conformation outside the binding pocket is likely an artifact of the TMD method.

*Figure 15*

*here*

### **Binding of AA<sub>t</sub>**

The results of the AA<sub>t</sub> simulations presented in Fig. 14b,d differ from the AA case both in regard to force profile as well as C20 position. The forces necessary to move the fatty acid in the channel are higher for AA<sub>t</sub> than for AA; only at the end of the binding process (>

40 ps) is this situation inverted. The reason for the latter is that  $AA_t$  enters the binding pocket in a manner similar to the inversion of the unbinding trajectory while AA requires a large conformational change at the end of the binding process, since it enters the binding pocket with its tail first (Fig. 15).

The reason for the difference in the behavior of AA and  $AA_t$  in the TMD simulations lies in the inability of the *trans* isomer to carry out small amplitude concerted torsional motions inside the binding pocket. The increased flexibility of AA allows the molecule to adapt itself easily to the constraints imposed by the narrow COX channel.

## Conclusions

Different pathways of acquiring AA for the COX reaction have been proposed (Otto and Smith, 1995; Herschman, 1996; Smith and DeWitt, 1996) but no direct experimental observations have been reported that detail how AA enters the COX channel of PGHS-1. PGHS-1 is mainly located on the luminal side of the endoplasmatic reticulum membrane (Smith and DeWitt, 1996). One of the sources for AA is the cleavage of phospholipids by phospholipase A<sub>2</sub> which acts on the cytoplasmic side of the membrane. AA is hydrophobic and once released from membrane phospholipids it presumably remains associated with the bilayer. The relatively fast rate of exchange for fatty-acids between leaflets of the lipid bilayer (Hamilton, 1998) allows AA to diffuse or to be transported from the cytoplasmic site to the luminal side of the membrane. On the luminal side AA will align in the more probable configuration along with the phospholipids, its carboxyl head pointing towards the aqueous phase.

Possible scenarios for AA binding based on the results of our SMD and TMD simulations are presented in Fig. 16. Initial binding of AA to PGHS-1 probably occurs by the interaction of the carboxylate head of AA with Arg83 which is one of the polar groups in the hydrophobic membrane binding motif anchoring PGHS-1 to the phospholipid headgroups (cf., Fig. 16b). Arg83 can adopt two configurations and the switch from the membrane binding conformation to the alternate conformation shown in Fig. 16c effectively shuttles an attached AA molecule from the membrane to the entrance of the COX site. Arg83 in its alternate conformation binds Glu524, which in turn releases Arg120. Arg120 in turn is free to take over the binding of AA from Arg83 (cf., Fig. 16d). Alternatively, if Arg83 is

bound to Glu524 initially, Arg120 “picks up” the carboxylate head of AA emerging from the bilayer (cf., Fig. 16a). The role of Arg83 in PGHS-1 could be tested by mutation experiments. Water present at the mouth of the binding channel might mediate this sequence of events by destabilizing the strong electrostatic interactions between the AA carboxylate group and the Arg guanido groups.

*Figure 16*

Being shuttled to the mouth of the COX channel AA has essentially two possibilities to enter. Most likely AA adopts an extended conformation and will enter the binding pocket with its tail last (cf., Fig. 16e,f). Except for the two arginines (Arg83 and Arg120), no large scale conformational changes in the protein itself were observed during the binding/unbinding process. The dominant motions, as revealed through ED analysis, occur in the fatty acid. AA is able to pass the protein residues that line the channel without the need of large side-chain reorientations. The interaction with the fatty acid mostly results in rotations of terminal methyl groups in the hydrophobic residues.

*here*

From both the SMD and TMD simulations the all-*cis* structure of AA emerges as optimal for finally achieving an orientation in the channel necessary for the COX reaction. Concerted rotations of dihedral angles in the fatty acid occur as it moves inside the COX channel and the arrangement of double bonds separated by two single bonds is optimal for efficient entrance to and exit from the channel. The selectivity of PGHS for AA results from the high degree of motional flexibility associated with concerted torsional motions specific for alternating *cis* double bond - single bond - single bond chains. As a result of this selectivity a fatty acid could be a poor COX substrate, or an effective inhibitor, because it does not have the suitable arrangement of bonds either for movement into the channel or for adopting the U-shape necessary for the COX chemistry to occur. This selection mechanism can explain

why for example only fair cyclooxygenation occurs with  $\gamma$ -linolenic acid,  $\alpha$ -linolenic acid, and linolenic acid. These fatty acids have a reduced number (two or three) of *cis* double bonds, which leads to a reduction in the binding rate. Docosahexaenoic acid (22:6 $\omega$ 3) on the other hand has a suitable structure for entering the binding pocket (six *cis* double bonds), but the configuration of double bonds is not oriented favorably for the COX reaction which may explain why this fatty acid is an efficient competitive PGHS inhibitor (Smith and DeWitt, 1996).

The present studies should be extended in several different directions. A comparison with SMD and TMD simulations of PGHS-2 could reveal crucial differences for the selective inhibition of the two enzymes. Arg83, for example, is changed to Lys83 in PGHS-2 and the latter residue may not play the same role in PGHS-2 as Arg83 does in PGHS-1. One may also extend the present study adding the second monomer, part of the bilayer, and water. Finally, unbinding of inhibitors (NSAIDS) from the COX site (with known initial structure), could lay the foundation for free energy calculations and an understanding of the activity of these compounds.

## Acknowledgment

The authors thank D. Kosztin for helpful discussions and the initial system setup. The initial structure of PGHS-1 with AA in the COX channel was kindly provided by Dr. R. M. Garavito. This work was supported by grants from the National Institutes of Health (PHS 5 P41 RR05969-04), the National Science Foundation (BIR-9318159, BIR 94-23827 EQ), the Roy J. Carver Charitable Trust, and by the MCA 93S028P computer time grant at Pittsburgh Supercomputing Center. The figures in this paper were created with the molecular graphics program VMD (Humphrey *et al.*, 1996) (<http://www.ks.uiuc.edu/Research/VMD>).

## References

- Balsera, M., S. Stepaniants, S. Izrailev, Y. Oono, and K. Schulten. 1997. Reconstructing potential energy functions from simulated force-induced unbinding processes. *Biophys. J.* 73:1281–1287.
- Bernstein, F. C., T. F. Koetzle, G. J. Williams, E. F. Meyer, M. D. Brice, J. R. Rogers, O. Kennard, T. Shimanouchi, and M. Tasumi. 1977. The Protein Data Bank: A computer-based archival file for macromolecular structures. *J. Mol. Biol.* 112:535–542.
- Brooks, B. R., R. E. Bruccoleri, B. D. Olafson, D. J. States, S. Swaminathan, and M. Karplus. 1983. CHARMM: A program for macromolecular energy, minimization, and dynamics calculations. *J. Comp. Chem.* 4:187–217.
- Brünger, A. T. 1992. *X-PLOR, version 3.1: A system for X-ray crystallography and NMR*. New Haven and London: Yale University Press.
- Callan, O. H., O.-Y. So, and D. C. Swinney. 1996. The Kinetic Factors That Determine the Affinity and Selectivity for Slow Binding Inhibition of Human Prostaglandin H Synthase 1 and 2 by Indomethacin and Flurbiprofen. *J. Biol. Chem.* 271(7):3548–3554.
- Frisch, M. J., G. W. Trucks, H. B. Schlegel, P. M. W. Gill, B. G. Johnson, M. A. Robb, J. R. Cheeseman, T. Keith, G. A. Petersson, J. A. Montgomery, K. Raghavachari, M. A. Al-Laham, V. G. Zakrzewski, J. V. Ortiz, J. B. Foresman, C. Y. Peng, P. Y. Ayala, W. Chen, M. W. Wong, J. L. Andres, E. S. Replogle, R. Gomperts, R. L. Martin, D. J. Fox, J. S. Binkley, D. J. Defrees, J. Baker, J. P. Stewart, M. Head-Gordon, C. Gonzalez, and J. A. Pople. 1995. *Gaussian 94, revision b.3*. Gaussian Inc., Pittsburgh, PA.

- Grubmüller, H., B. Heymann, and P. Tavan. 1996. Ligand binding and molecular mechanics calculation of the streptavidin-biotin rupture force. *Science* 271:997–999.
- Hamilton, J. 1998. Fatty acid transport: difficult or easy? *J. Lipid. Res.* 39(3):467–481.
- Heller, H., M. Schaefer, and K. Schulten. 1993. Molecular dynamics simulation of a bilayer of 200 lipids in the gel and in the liquid crystal-phases. *J. Phys. Chem.* 97:8343–8360.
- Hermans, J., G. Mann, L. Wang, and L. Zhang. 1998. Simulation studies of protein-ligand interactions. *In: Deuffhard, P., J. Hermans, B. Leimkuhler, A. Mark, R. D. Skeel, and S. Reich (eds), Computational molecular dynamics: Challenges, methods, ideas.* Lecture Notes in Computational Science and Engineering. Springer-Verlag. In press.
- Herschman, H. 1996. Prostaglandin synthase 2. *Biochim. Biophys. Acta* 1299:125–140.
- Humphrey, W. F., A. Dalke, and K. Schulten. 1996. VMD – Visual Molecular Dynamics. *J. Mol. Graphics* 14:33–38.
- Israilewitz, B., S. Izrailev, and K. Schulten. 1997. Binding pathway of retinal to bacterio-opsin: A prediction by molecular dynamics simulations. *Biophys. J.* 73:2972–2979.
- Izrailev, S., S. Stepaniants, M. Balsera, Y. Oono, and K. Schulten. 1997. Molecular dynamics study of unbinding of the avidin-biotin complex. *Biophys. J.* 72:1568–1581.
- Izrailev, S., S. Stepaniants, B. Israilewitz, D. Kosztin, H. Lu, F. Molnar, W. Wriggers, and K. Schulten. 1998. Steered molecular dynamics. *Pages 39–65 of: Deuffhard, P., J. Hermans, B. Leimkuhler, A. E. Mark, S. Reich, and R. D. Skeel (eds), Computational molecular dynamics: Challenges, methods, ideas.* Lecture Notes in Computational Science and Engineering, vol. 4. Berlin: Springer-Verlag.

- Kalgutkar, A. S., B. C. Crews, S. W. Rowlinson, C. Garner, K. Seibert, and L. J. Marnett. 1998. Aspirin-like Molecules that Covalently Inactivate Cyclooxygenase-2. *Science* 280:1268–1270.
- Kosztin, D., S. Izrailev, and K. Schulten. 1999. Unbinding of retinoic acid from its receptor studied by steered molecular dynamics. *Biophys. J.* 76:188–197.
- Kurumbail, R. G., A. M. Stevens, J. K. Gierse, J. J. McDonald, R. A. Stegeman, J. Y. Pak, D. Gildehaus, J. M. Miyashiro, T. D. Penning, K. Seibert, P. C. Isakson, and W. C. Stallings. 1996. Structural basis for selective inhibition of cyclooxygenase-2 by anti-inflammatory agents. *Nature* 348(6610):644–648.
- Leech, J., J. Prins, and J. Hermans. 1996. SMD: Visual steering of molecular dynamics for protein design. *IEEE Comp. Sci. & Eng.* 3(4):38–45.
- Lu, H., B. Isralewitz, A. Krammer, V. Vogel, and K. Schulten. 1998. Unfolding of titin immunoglobulin domains by steered molecular dynamics simulation. *Biophys. J.* 75:662–671.
- Lüdemann, S. K., O. Carugo, and R. C. Wade. 1997. Substrate access to cytochrome P450cam: A comparison of a thermal motion pathway analysis with molecular dynamics simulation data. *J. Mol. Model.* 3:369–374.
- Luong, C., A. Miller, J. Barnett, J. Chow, C. Ramesha, and M. F. Browner. 1996. Flexibility of the NSAID binding site in the structure of human cyclooxygenase-2. *Nature Struct. Biol.* 3(11):927–933.

- Ma, J., and M. Karplus. 1997. Molecular switch in signal transduction: Reaction paths of the conformational changes in *ras* p21. *Proc. Natl. Acad. Sci. USA* 94:11905–11910.
- MacKerell Jr., A. D., J. Wiorkiewicz-Kuczera, and M. Karplus. 1995. An all-atom empirical energy function for the simulation of nucleic acids. *J. Am. Chem. Soc.* 117(48):11946–11975.
- Marrink, S.-J., O. Berger, P. Tieleman, and F. Jähnig. 1998. Adhesion forces of lipids in a phospholipid membrane studied by molecular dynamics simulations. *Biophys. J.* 74:931–943.
- Masferrer, J., P. Isakson, and K. Seibert. 1996. Cyclooxygenase-2 Inhibitors. *NSAIDs, Eicosanoids, and the Gastroenteric Tract* 25(2):363–372.
- Nelson, M., W. Humphrey, A. Gursoy, A. Dalke, L. Kalé, R. D. Skeel, and K. Schulten. 1996. NAMD – A parallel, object-oriented molecular dynamics program. *Int. J. Supercomput. Appl. High Perform. Comput.* 10:251–268.
- Otto, J. C., and W. L. Smith. 1995. Prostaglandin endoperoxide synthase-1 and -2. *J. Lipid Mediators Cell Signalling* 12:139–156.
- Picot, D., P. J. Loll, and M. Garavito. 1994. The X-ray crystal structure of the membrane protein prostaglandin  $H_2$  synthase-1. *Nature* 367(20):243–249.
- Picot, R., and R. M. Garavito. 1994. Prostaglandin H synthase: implications for membrane structure. *FEBS Lett.* 346(1):21–25.

- Schlitter, J., M. Engels, P. Krüger, E. Jacoby, and A. Wollmer. 1993. Targeted molecular dynamics simulation of conformational change - application to the T  $\leftrightarrow$  R transition in insulin. *Molecular Simulation* 10(2-6):291-308.
- Schreiber, J., T. Eling, and R. Mason. 1986. The oxidation of arachidonic acid by the cyclooxygenase activity of purified prostaglandin H synthase: spin trapping of a carbon-centered free radical intermediate. *Arch. Biochem. Biophys.* 249(1):126-136.
- Smith, W. L., and D. L. DeWitt. 1995. Biochemistry of prostaglandin H synthase-1 and synthase-2 and their differential susceptibility to nonsteroidal anti-inflammatory drugs. *Seminars in Nephrology* 15(3):179-194.
- Smith, W., and D. DeWitt. 1996. Prostaglandin endoperoxide H synthases-1 and -2. *Adv. Immunol.* 62:167-215.
- Smith, W., R. Garavito, and D. DeWitt. 1996. Prostaglandin Endoperoxide H Synthases (Cyclooxygenases)-1 and -2. *J. Biol. Chem.* 271(52):33157-33160.
- So, O.-Y., L. E. Scarafia, A. Y. Mak, O. H. Callan, and D. C. Swinney. 1998. The Dynamics of Prostaglandin H Synthases. *J. Biol. Chem.* 273(10):5801-5807.
- Stepaniants, S., S. Izrailev, and K. Schulten. 1997. Extraction of lipids from phospholipid membranes by steered molecular dynamics. *J. Mol. Model.* 3:473-475.
- Swinney, D. C., A. Y. Mak, J. Barnett, and C. S. Ramesha. 1997. Differential Allosteric Regulation of Prostaglandin H Synthase 1 and 2 by Arachidonic Acid. *J. Biol. Chem.* 272(19):12393-12398.

- Tsai, A., R. Kulmacz, and G. Palmer. 1995. Spectroscopic evidence for reaction of prostaglandin H synthase-1 tyrosyl radical with arachidonic acid. *J. Biol. Chem.* 270(18):10503–10508.
- Tsai, A., G. Palmer, G. Xiao, D. Swinney, and R. Kulmacz. 1998. Structural Characterization of Arachidonyl Radicals Formed by Prostaglandin H Synthase-2 and Prostaglandin H Synthase-1 Reconstituted with Mangano Protoporphyrin IX. *J. Biol. Chem.* 273(7):3888–3894.
- van Aalten, D. M. F., B. L. de Groot, H. Berendsen, and J. B. C. Findlay. 1996. Conformational analysis of retinoids and restriction of their dynamics by retinoid-binding proteins. *Biochem. J.* 319:543–550.
- Wiener, M. C., and S. H. White. 1992. Structure of a fluid dioleoylphosphatidylcholine bilayer determined by joint refinement of x-ray and neutron diffraction data; III. complete structure. *Biophys. J.* 61(Feb.):434–447.
- Wu, X., and S. Wang. 1998. Self-Guided Molecular Dynamics Simulation for Efficient Conformational Search. *J. Phys. Chem. B* 102(37):7238–7250.

---

Table 1: SMD unbinding steps of AA (cf., Fig. 5a,d).

---

Step	Description
0-150 ps	initial phase of a slowly increasing force interrupted
(1) and (2)	by a small decrease in force around 90 ps
150-230 ps	the force reaches its maximum at about 500 pN and
(3) to (5)	drops back to 150 pN in four steps
> 230 ps	the force is increasing again because AA is pulled
(6)	further, but no more changes in position are observed; AA has exited from the binding channel and remains strongly bound to Arg120 in an extended conformation

---

Table 1:

---

Table 2: SMD unbinding steps of  $AA_t$  (cf., Fig. 5b,e).

---

Step	Description
0-40 ps	a phase of a slowly increasing force is preceded by a sharp increase and slow decay of the force
40-210 ps	the force is slowly increasing until it reaches a peak value of 650 pN
(1)	
210-260 ps	the force drops to 100 pN in three stages
(4) and (5)	
> 260 ps	the force is growing again, but no further changes in position are observed as $AA_t$ has been pulled out completely from its binding pocket and remains strongly bound to Arg120
(6)	

---

Table 2:

---

Table 3: SMD unbinding steps of AA<sub>s</sub> (cf., Fig. 5c,f).

---

Step	Description
40-100 ps	the force increases until it reaches a value of
(1)	200 pN and drops back to 100 pN
100-220 ps	the force increases again, reaches a peak value
(2) and (3)	of 550 pN, but experiences at 200 ps an intermediate drop to 450 pN
> 220 ps	the force increases again since AA <sub>s</sub> has not
(5)	fully exited the binding pocket after 300 ps

---

Table 3:

---

Table 4: ED analysis of SMD unbinding steps of AA (cf., Figs. 9 and 10).

---

Time [ps]	Description
35-41	the tail of AA moves towards the exit of the binding channel and interacts with the residues forming the doorway, as reflected by localized large amplitudes of H atoms at the end of the fatty acid tail
74-81	reorientation of the carboxylate head region
89-95	concerted motion near C8=C9, C11=C12, and C14=C15
148-150	first main unbinding event, in the form of concerted rotation near C8=C9
171-172	tail region has exited binding channel and undergoes large amplitude motions
191-193	second main unbinding event, involves concerted rotations near C5=C6
222-224	final exit from binding pocket involving translational motion of the tail and rotations around single bonds between C4 and the carboxylate head

---

Table 4:

---

Table 5: SMD unbinding steps of AA with ten water molecules added at the mouth of the COX binding channel (cf., Fig. 12)

---

Step	Description
0-100 ps	reorientation of fatty acid chain involving mainly
(1) → (3)	the region around the C11=C12 double bond
100-200 ps	main unbinding event involving torsions near
(4) → (5)	C8=C9 and C5=C6
220-290 ps	rotation around single bonds between C4 and the
(5)	carboxylate head

---

Table 5:

## Figure Captions

**Figure 1:** Structure of ovine PGHS-1 homo dimer (Picot *et al.*, 1994). One monomeric subunit is depicted in a cartoon/ribbon representation, amino acids of the other subunit are shown in a line representation. The heme groups are represented as a “licorice” model (green) in both subunits. Color codes: EGF domain - gold, membrane-binding helices (A-D) - red, globular domain - silver. AA is shown in its putative COX binding site in the right monomer (blue). Residues lining the hydrophobic COX channel in the globular part of PGHS-1 are presented in the monomer on the left (blue). The approximate location of one leaflet of the membrane bilayer is indicated by a dot-dashed line and single lipid molecules (red).

**Figure 2:** Equilibrated structure of the COX binding site of PGHS-1 with AA substrate. Residues at the bottom of the NSAID binding site (Arg120, Tyr355, Glu524) form a hydrogen bonding network and can switch conformations providing the substrate access to the COX site. The inset shows the chemical structure of AA with the adopted numbering scheme of its C atoms. AA is folded into the COX channel with a “kink” near C10.

**Figure 3:** Equilibrated structure of the COX binding site of PGHS-1 with (a) an 8-*trans* AA ( $AA_t$ ) and (b) an AA isomer with a single bond at the 8 position ( $AA_s$ ). The overall structure of the channel is very similar to the case where AA is bound (cf., Fig. 2), however, the fatty-acid tails of bound  $AA_t$  and bound  $AA_s$  adopt different conformations compared to bound AA.

**Figure 4:** Residues forming the “doorway” to the COX site in PGHS-1. Panel a: amino acid residues are displayed in van der Waals representation; AA (shown with hydrogens) is visible through an opening into the binding site; the pulling direction is approximately perpendicular to the plane containing Arg120, Tyr355, Val116, and Met113. Panel b: side-view of panel a; amino acid residues are presented without hydrogen atoms.

**Figure 5:** Comparison of force profiles and C20 atomic positions for SMD unbinding of AA, AA<sub>t</sub>, and AA<sub>s</sub>. Panel a: force profile for AA; panel b: force profile for AA<sub>t</sub>; panel c: force profile for AA<sub>s</sub>; panel d: displacement of C20 from original position for AA; panel e: displacement of C20 from original position for AA<sub>t</sub>; panel f: displacement of C20 from original position for AA<sub>s</sub>. The unbinding of the fatty acid occurs in distinct stages which are numbered for reference to Figs. 6, 7, Tables 1-3, and to the text. The numbering scheme adopted for AA<sub>t</sub> and AA<sub>s</sub> is the same as for AA in order to identify corresponding stages of unbinding; as a result certain numbers are skipped.

**Figure 6:** Correlated torsional motion near C5=C6 and C8=C9 as revealed by the time-dependence of dihedral angles (running averages over a 1 ps window). Panel a: C<sub>6</sub>-C<sub>7</sub>-C<sub>8</sub>=C<sub>9</sub> and C<sub>8</sub>=C<sub>9</sub>-C<sub>10</sub>-C<sub>11</sub> in AA; panel d: C<sub>3</sub>-C<sub>4</sub>-C<sub>5</sub>=C<sub>6</sub> and C<sub>5</sub>=C<sub>6</sub>-C<sub>7</sub>-C<sub>8</sub> in AA; panel b: C<sub>6</sub>-C<sub>7</sub>-C<sub>8</sub>=C<sub>9</sub> and C<sub>8</sub>=C<sub>9</sub>-C<sub>10</sub>-C<sub>11</sub> in AA<sub>t</sub>; panel e: C<sub>3</sub>-C<sub>4</sub>-C<sub>5</sub>=C<sub>6</sub> and C<sub>5</sub>=C<sub>6</sub>-C<sub>7</sub>-C<sub>8</sub> in AA<sub>t</sub>; panel c: C<sub>6</sub>-C<sub>7</sub>-C<sub>8</sub>-C<sub>9</sub> and C<sub>8</sub>-C<sub>9</sub>-C<sub>10</sub>-C<sub>11</sub> in AA<sub>s</sub>; panel f: C<sub>3</sub>-C<sub>4</sub>-C<sub>5</sub>=C<sub>6</sub> and C<sub>5</sub>=C<sub>6</sub>-C<sub>7</sub>-C<sub>8</sub> in AA<sub>s</sub>. The graphs for AA display correlated changes in dihedral angles while changes in dihedrals of AA<sub>t</sub> and AA<sub>s</sub> are largely uncorrelated (see text for details).

**Figure 7:** Torsional events occurring during the unbinding of AA from its COX binding site. The view is the same as in Fig. 4b; amino acid labels are omitted for clarity. Numbers on top of arrows correspond to the numbering scheme of Fig. 5 (see text for details).

**Figure 8:** ED analysis of motions in the COX binding site during the course of a SMD simulation. Atoms in light green have relatively high root total mean square deviations (RTMSD) while the atoms in dark orange have relatively low ones. RTMSD values are calculated by adding up the eigenvectors with the five largest eigenvalues weighted by the square root of their eigenvalues. The RTMSD value of Arg83 lies outside the chosen range and was set to zero. AA, shown in purple, is extracted along the direction indicated by the dashed arrow.

**Figure 9:** ED analysis of AA motion during unbinding (part1). The motions enabling transitions between stages of unbinding are correlated and localized. The structures in the middle of each row are starting structures. The two other structures at each time interval represent endpoints of the largest amplitude modes as revealed by ED. The localized amplitudes are proportional to the square root of the eigenvalue (RTMSD).

**Figure 10:** ED analysis of AA behavior during unbinding (part2). See Fig. 9 for details.

**Figure 11:** Switching the hydrogen bonding network at the entrance of the COX binding site in PGHS-1. After binding to Arg83, Glu524 severs the hydrogen bonds to Arg120 enabling large amplitude motions of the latter.

**Figure 12:** Unbinding of AA from PGHS-1 after ten water molecules have been added near the mouth of the COX channel (see text for details). The presence of water molecules widens the entrance to the binding site and AA is extracted more readily. Arg83 plays an important role in binding AA (see text).

**Figure 13:** Force profile (upper panel) and C20 position (lower panel) for PGHS-1 with AA and ten water molecules added at the mouth of the COX channel (see text). The SMD trajectory was continued until AA was completely detached from PGHS-1.

**Figure 14:** TMD unbinding of AA and AA<sub>t</sub>. Upper half: A translational motion is superimposed onto the unraveling of the fatty acid chain resulting in the exit of AA in a partially “folded” conformation. The snapshots correspond to the AA unbinding simulation (dashed line in panels a and c). The view is the same as in Fig. 4; amino acid labels are omitted for clarity. Lower half: Force profiles and C20 position plots for AA unbinding (panels a and c) and binding (panels b and d). Binding occurs faster than unbinding due to the reduced time scale specified for the TMD simulations.

**Figure 15:** Details of the TMD binding trajectory of AA. AA enters the binding pocket with its tail first, achieving the final bent conformation through a series of concerted rotations and a large scale conformational change at the end of the binding process. The view is the same as in Fig. 7b; amino acid labels are omitted for clarity.

**Figure 16:** Possible binding mechanisms. The electrostatic interaction between charged residues and the carboxylate head of AA guides the fatty acid towards the entrance of the COX active site (see text for details).

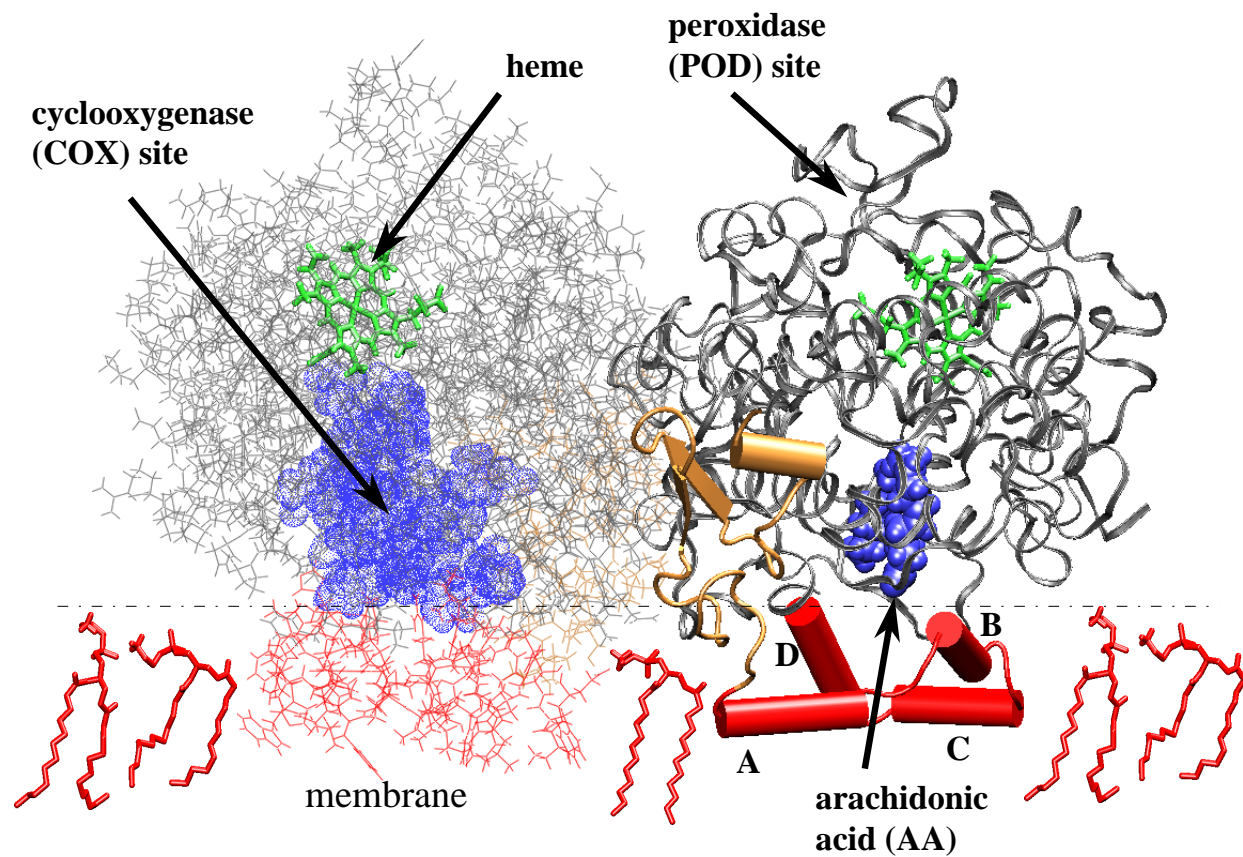


Figure 1:

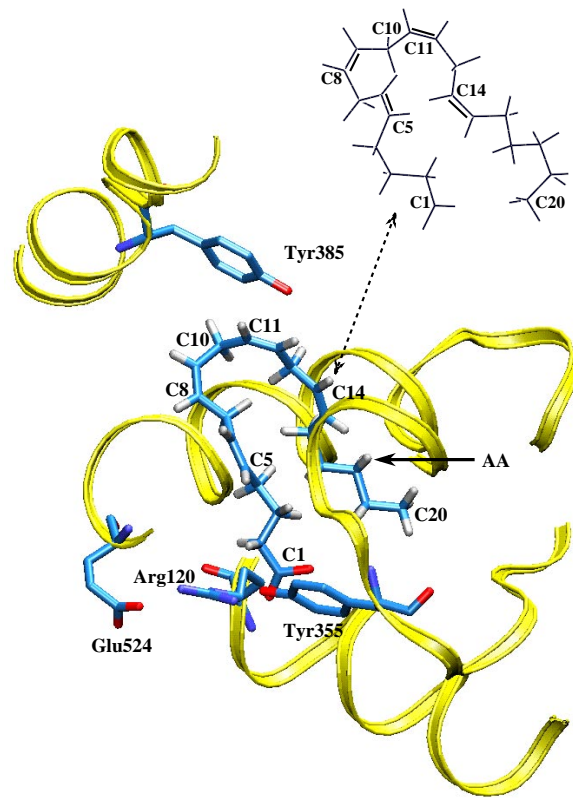


Figure 2:

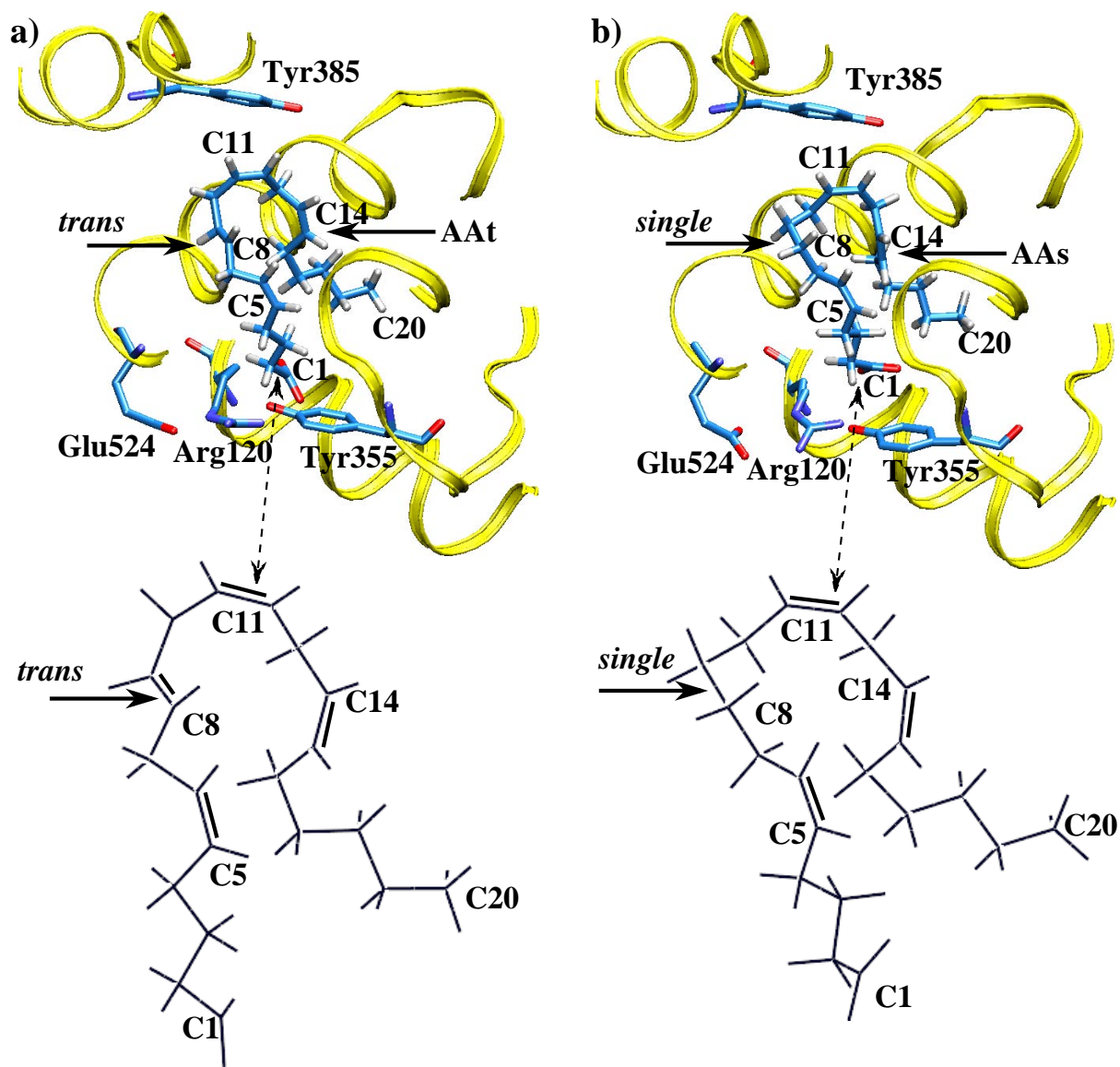


Figure 3:

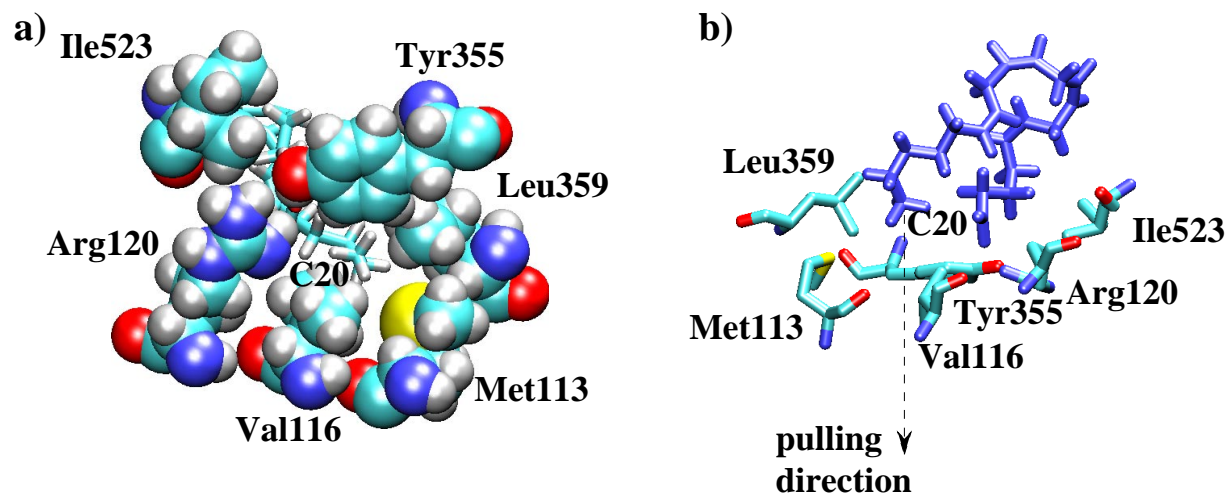


Figure 4:

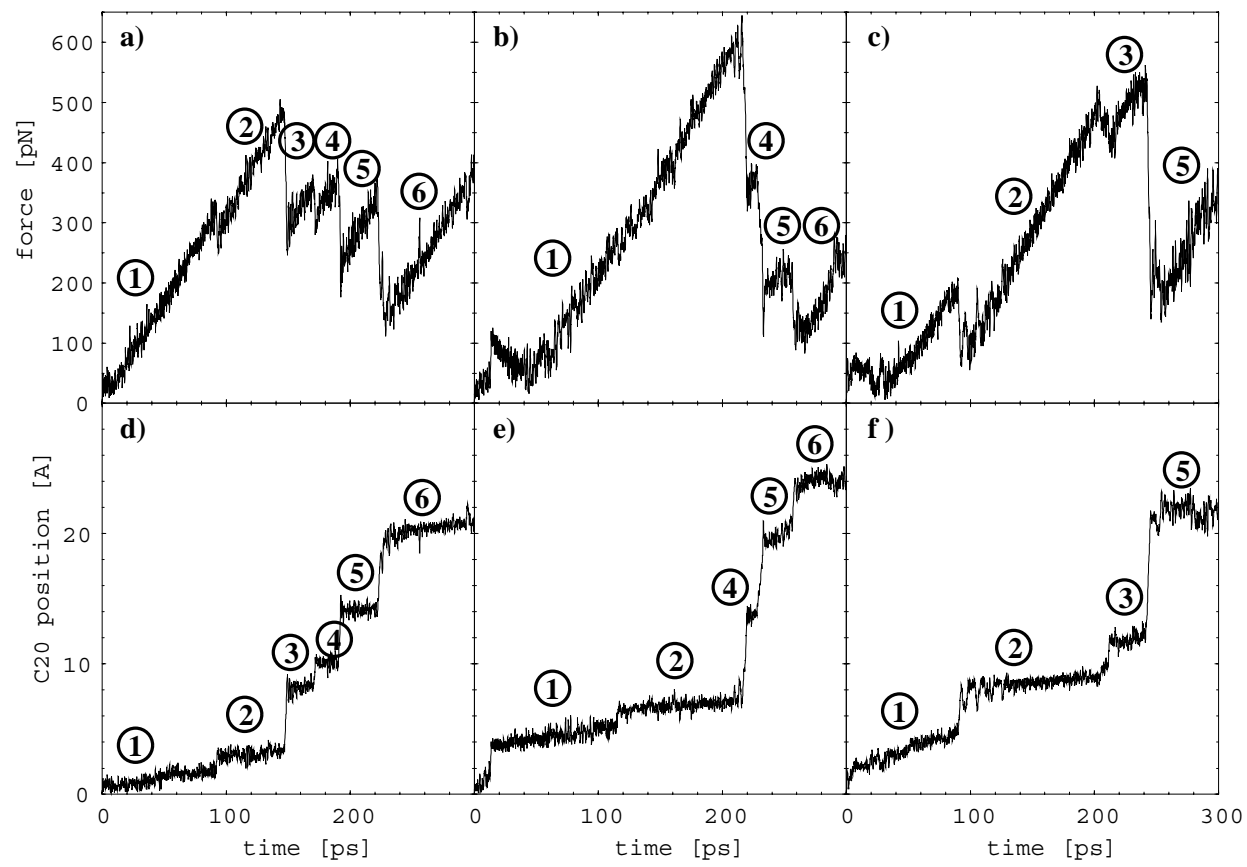


Figure 5:

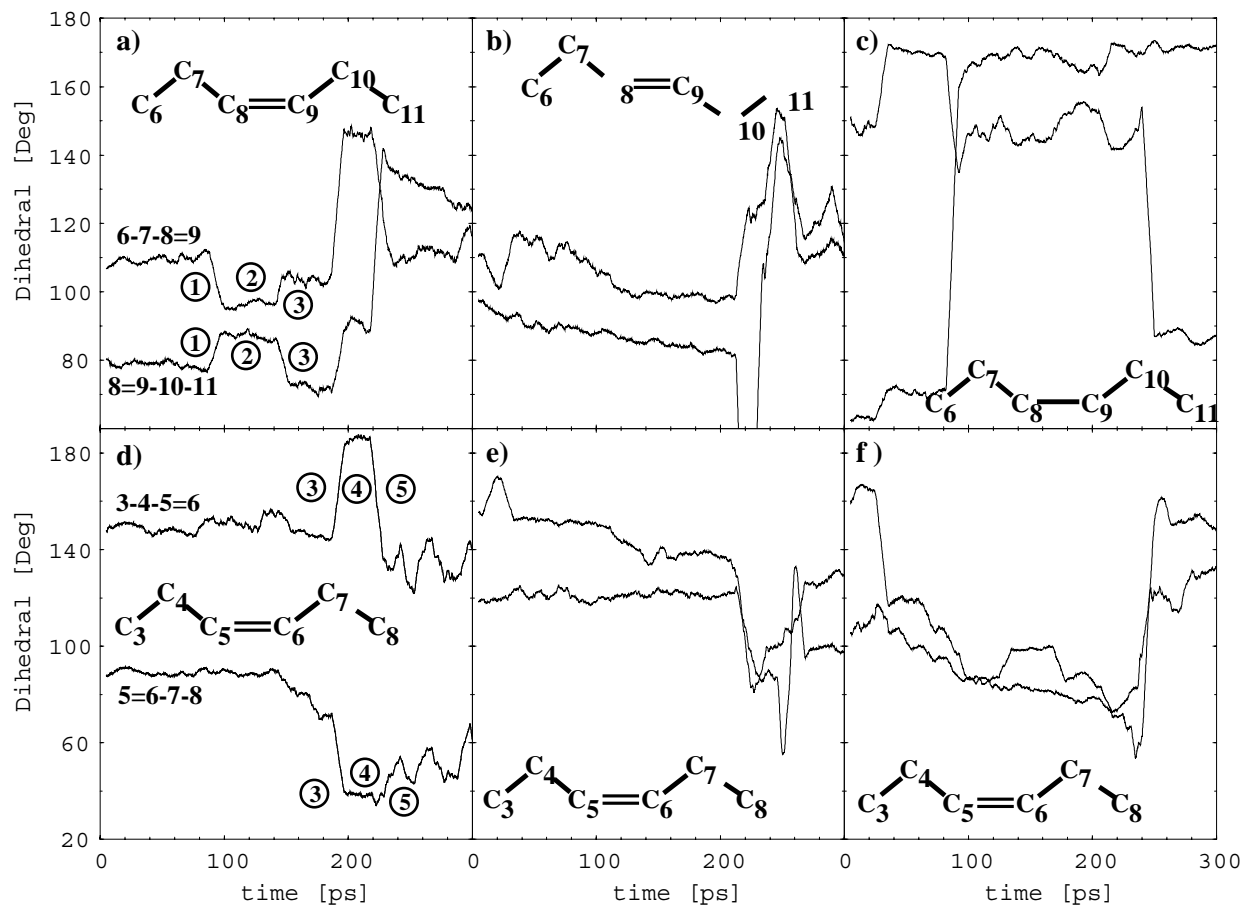


Figure 6:

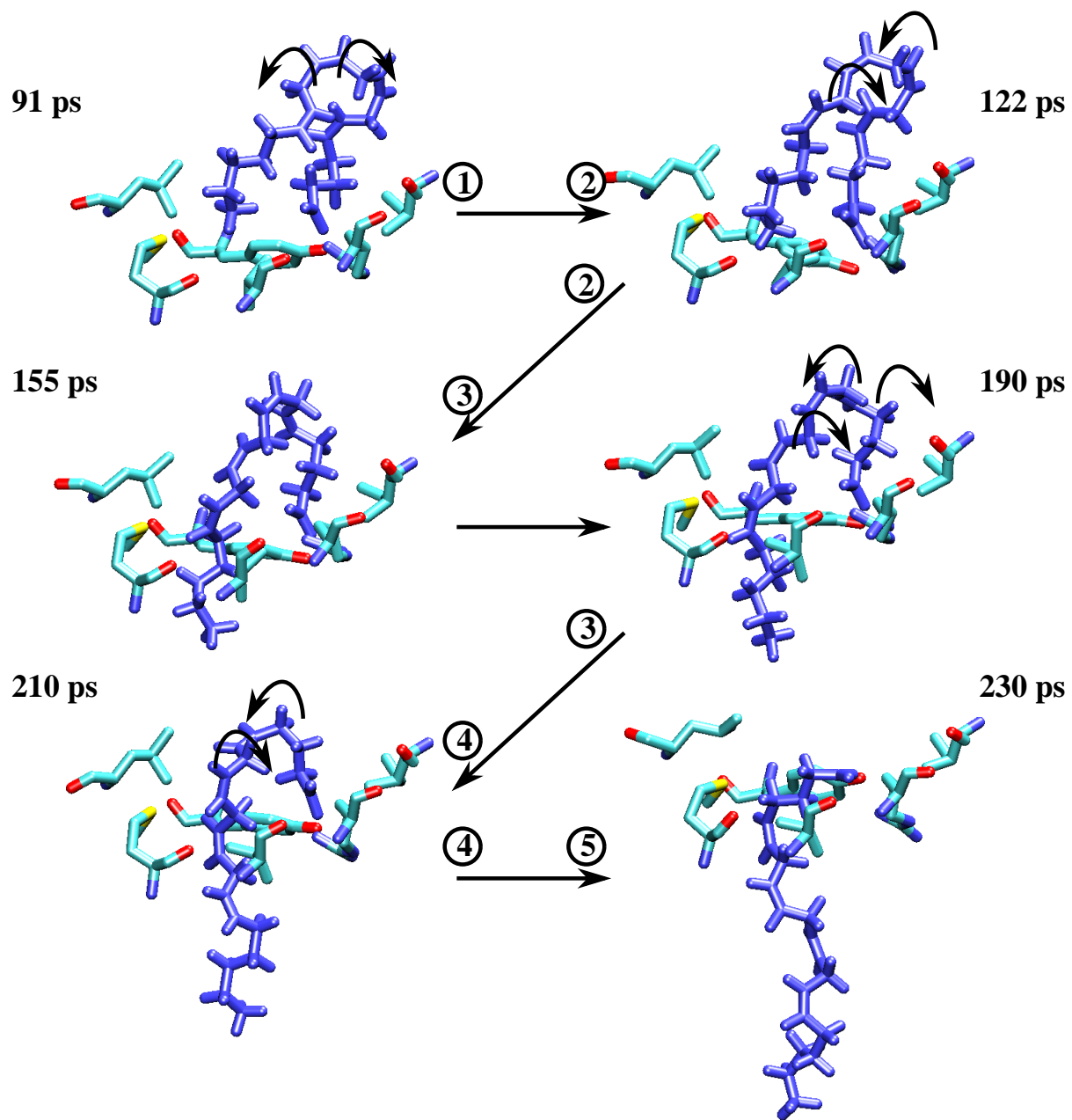


Figure 7:

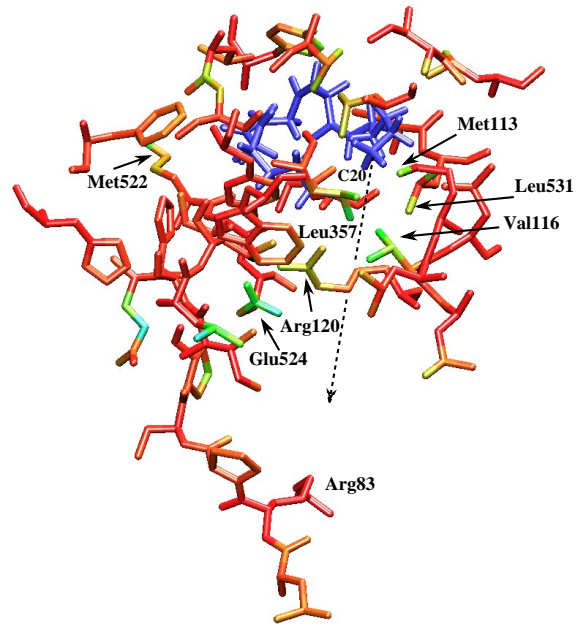
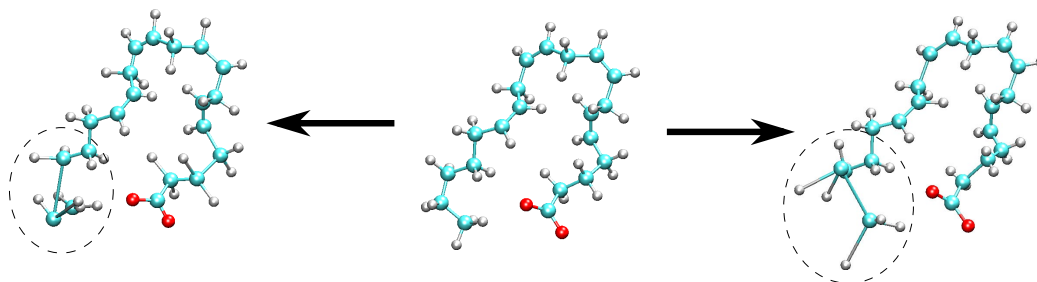
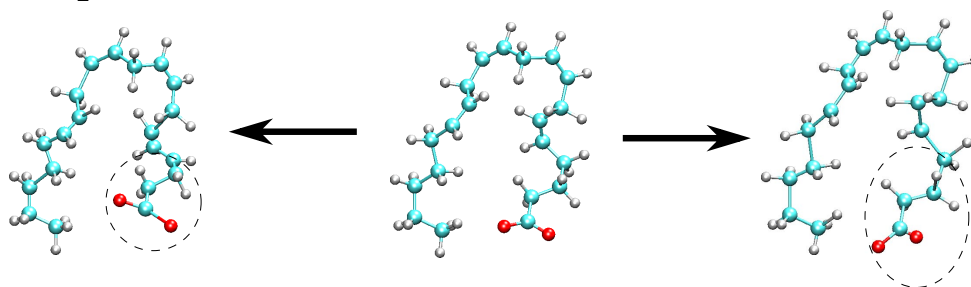


Figure 8:

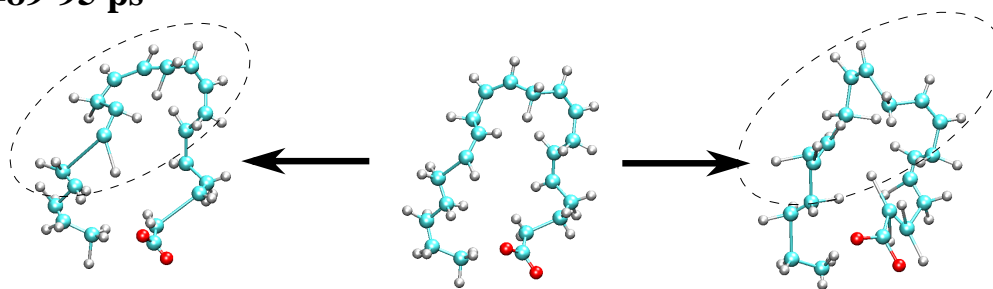
**t=35-41 ps**



**t=74-81 ps**



**t=89-95 ps**



**t=148-150 ps**

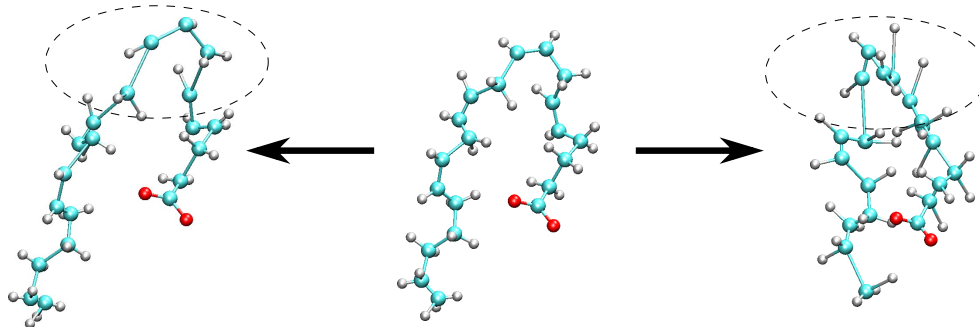
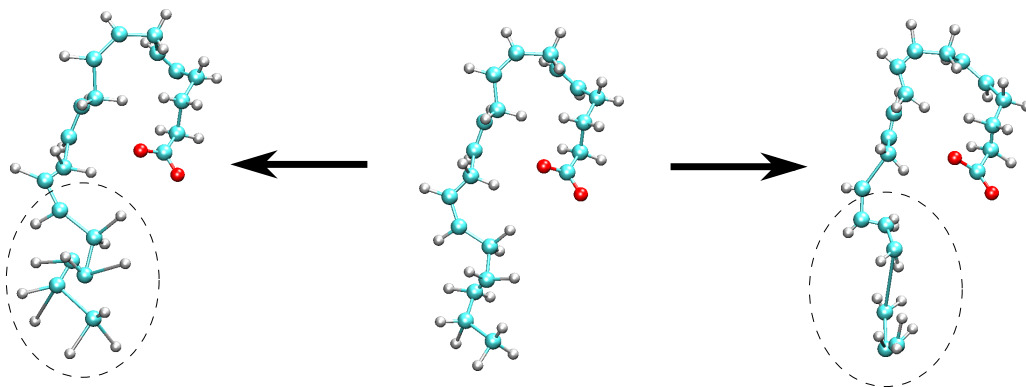
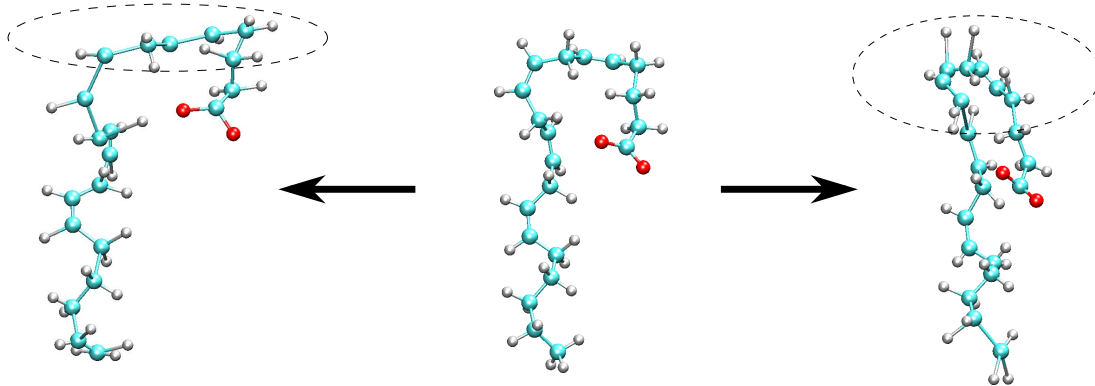


Figure 9:

**t=171-172 ps**



**t=191-193 ps**



**t=222-224 ps**

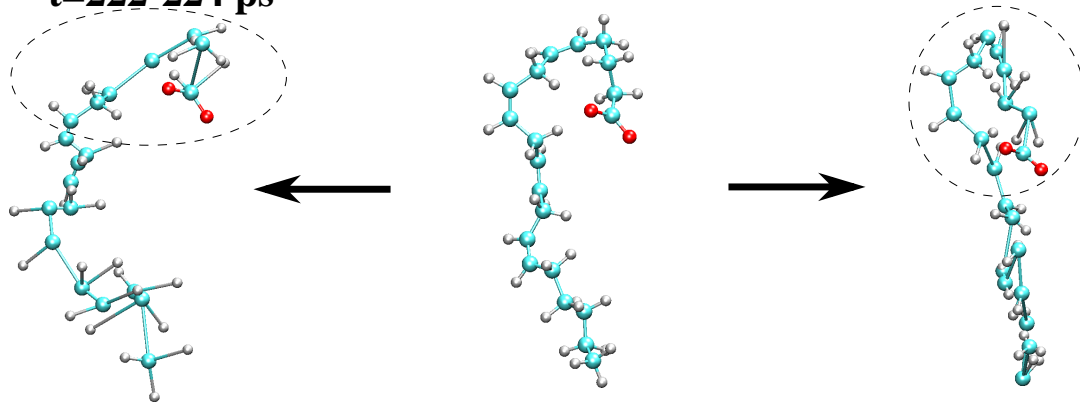


Figure 10:

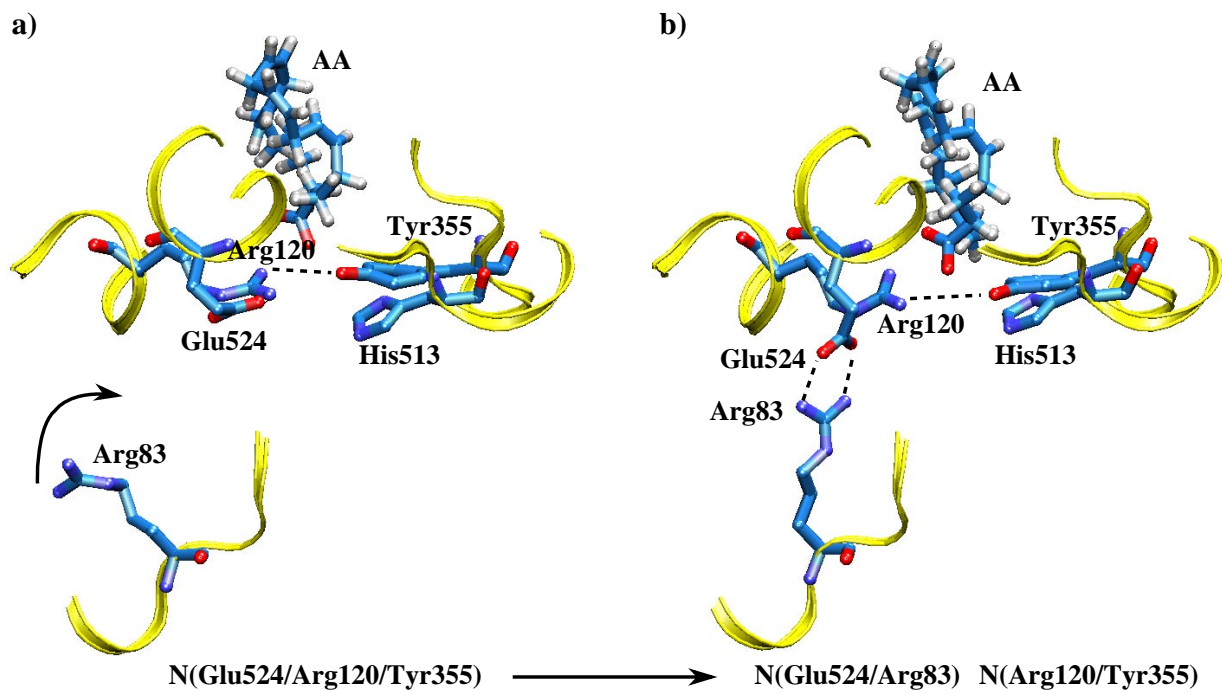


Figure 11:

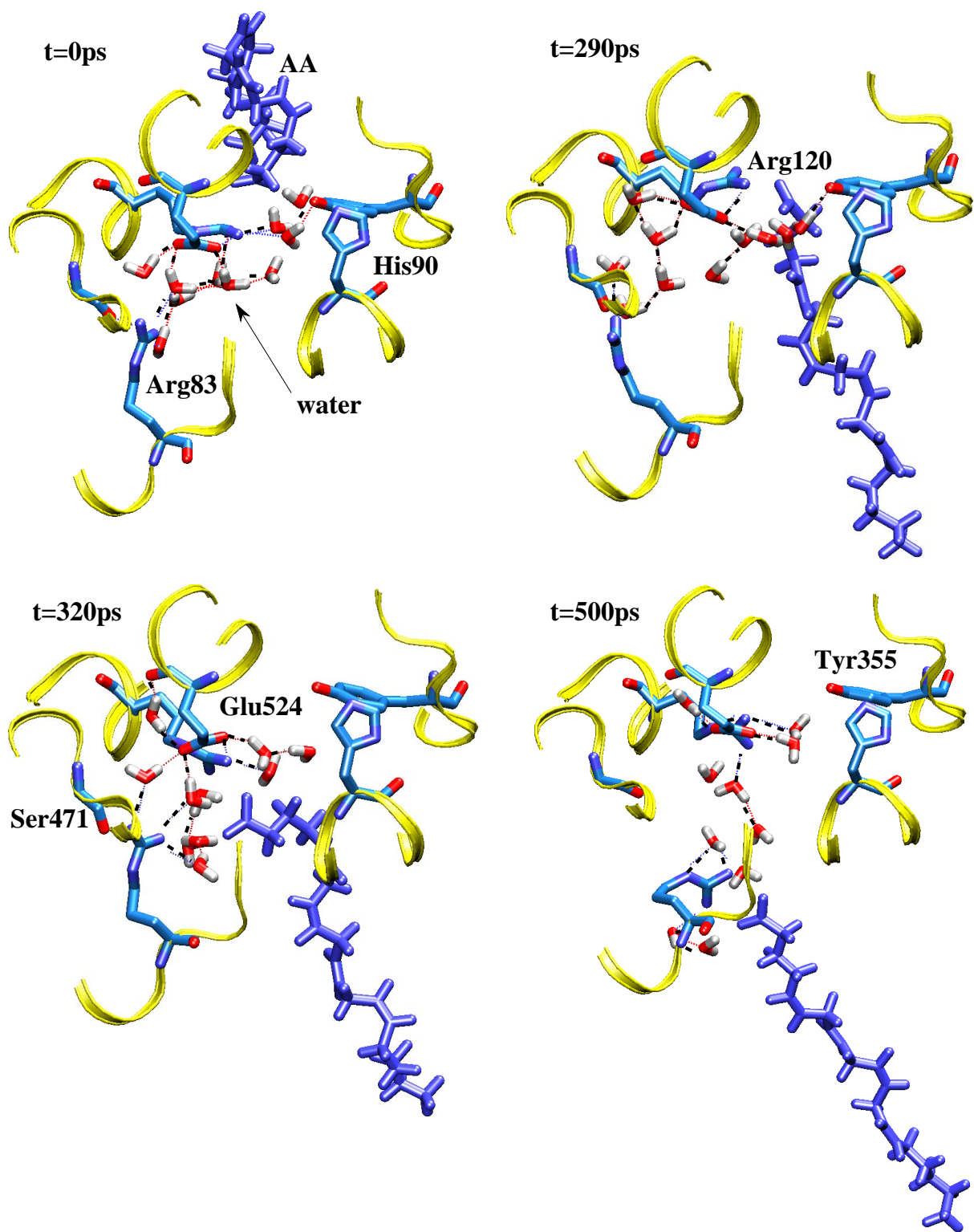


Figure 12:

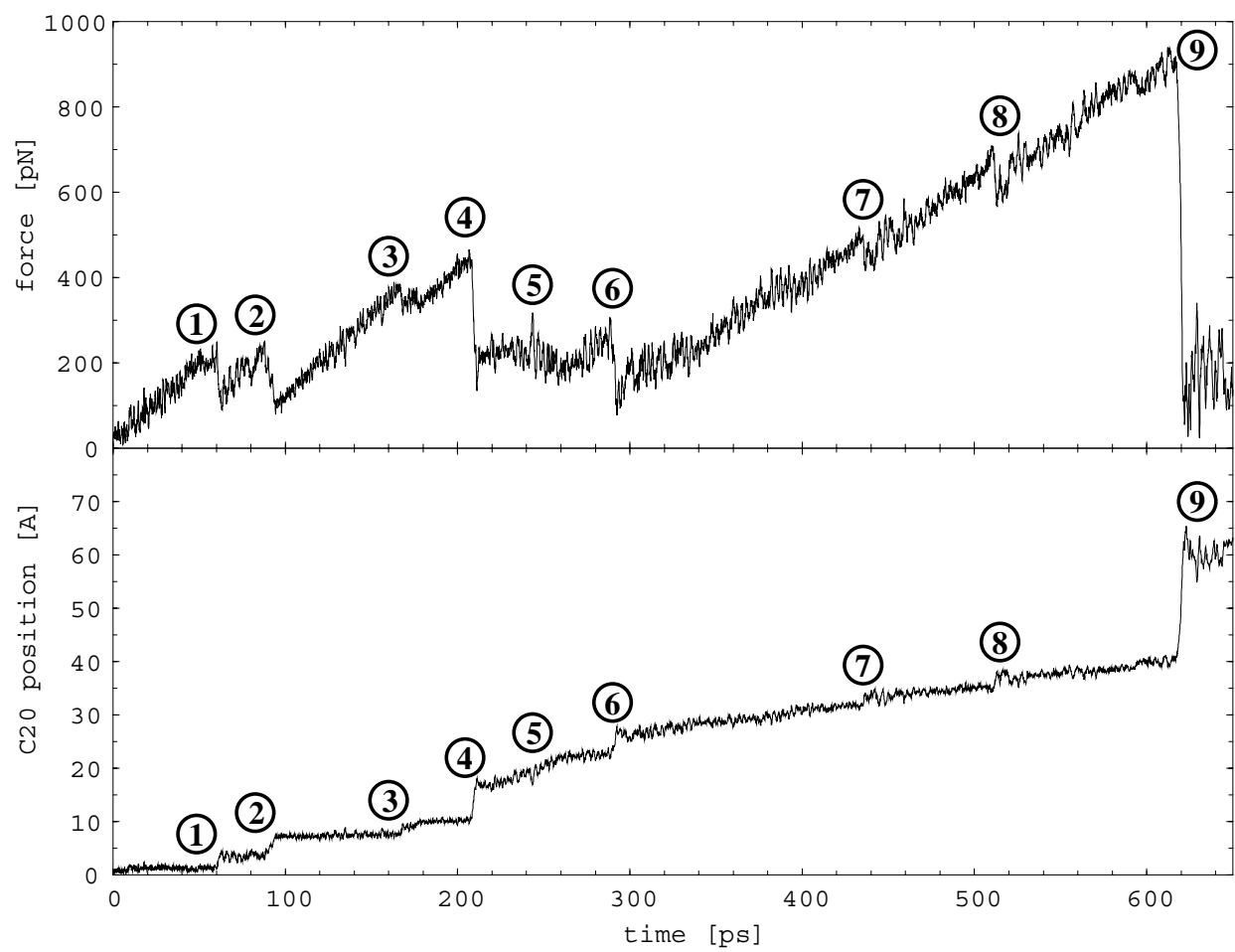


Figure 13:

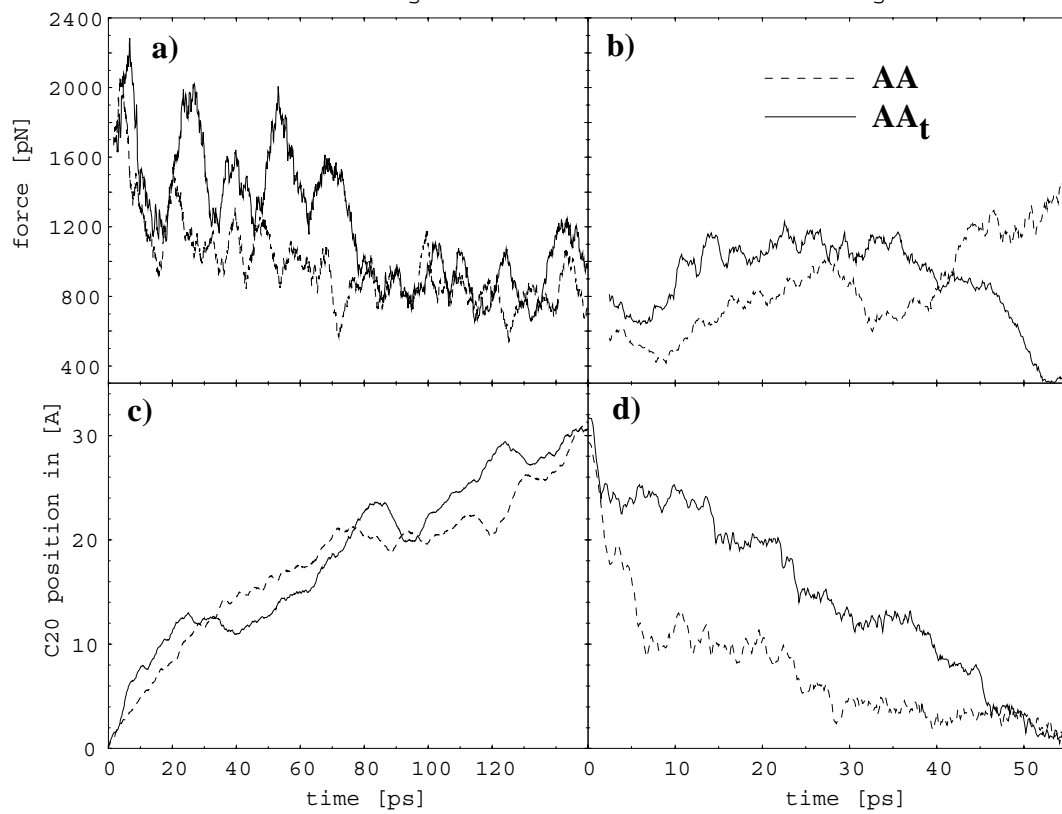
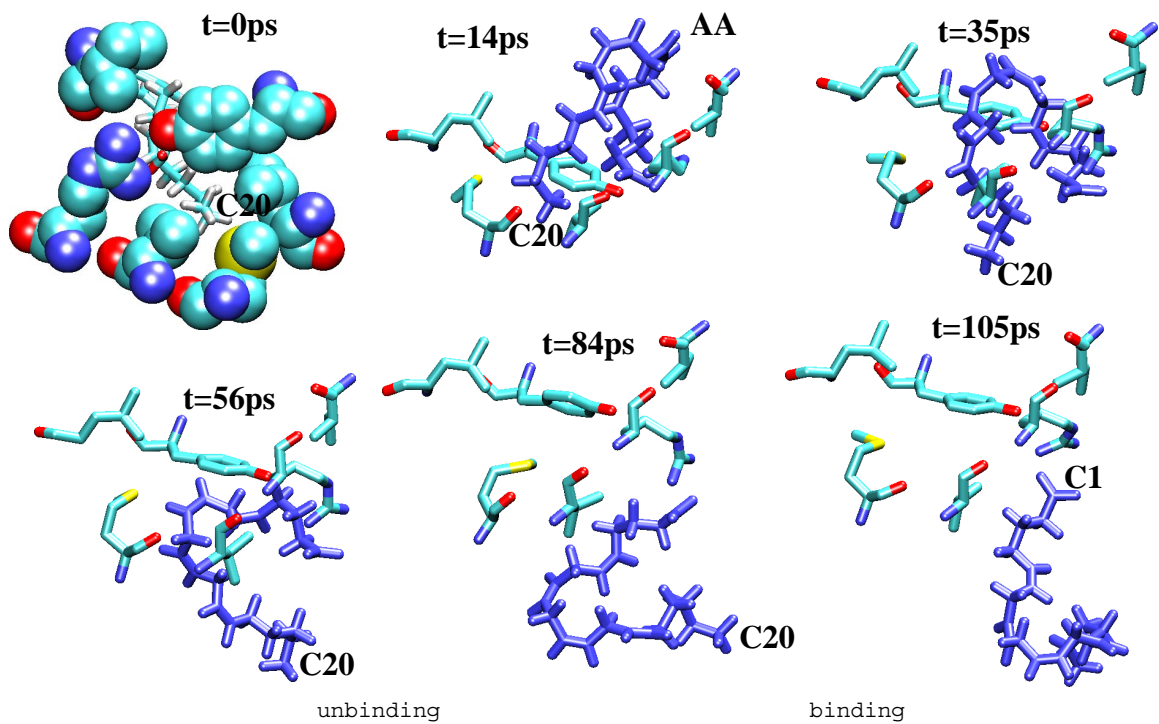


Figure 14:

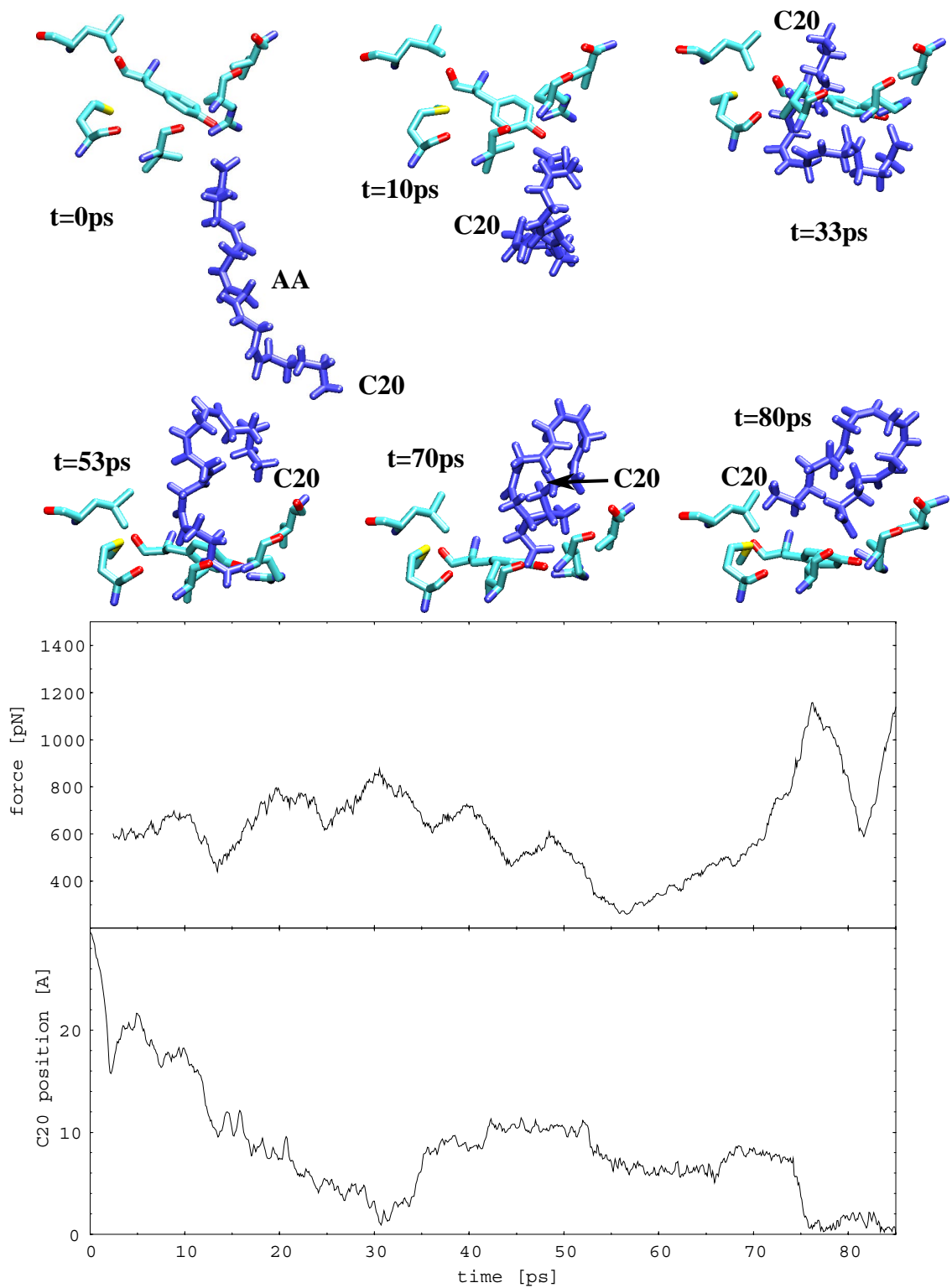


Figure 15:

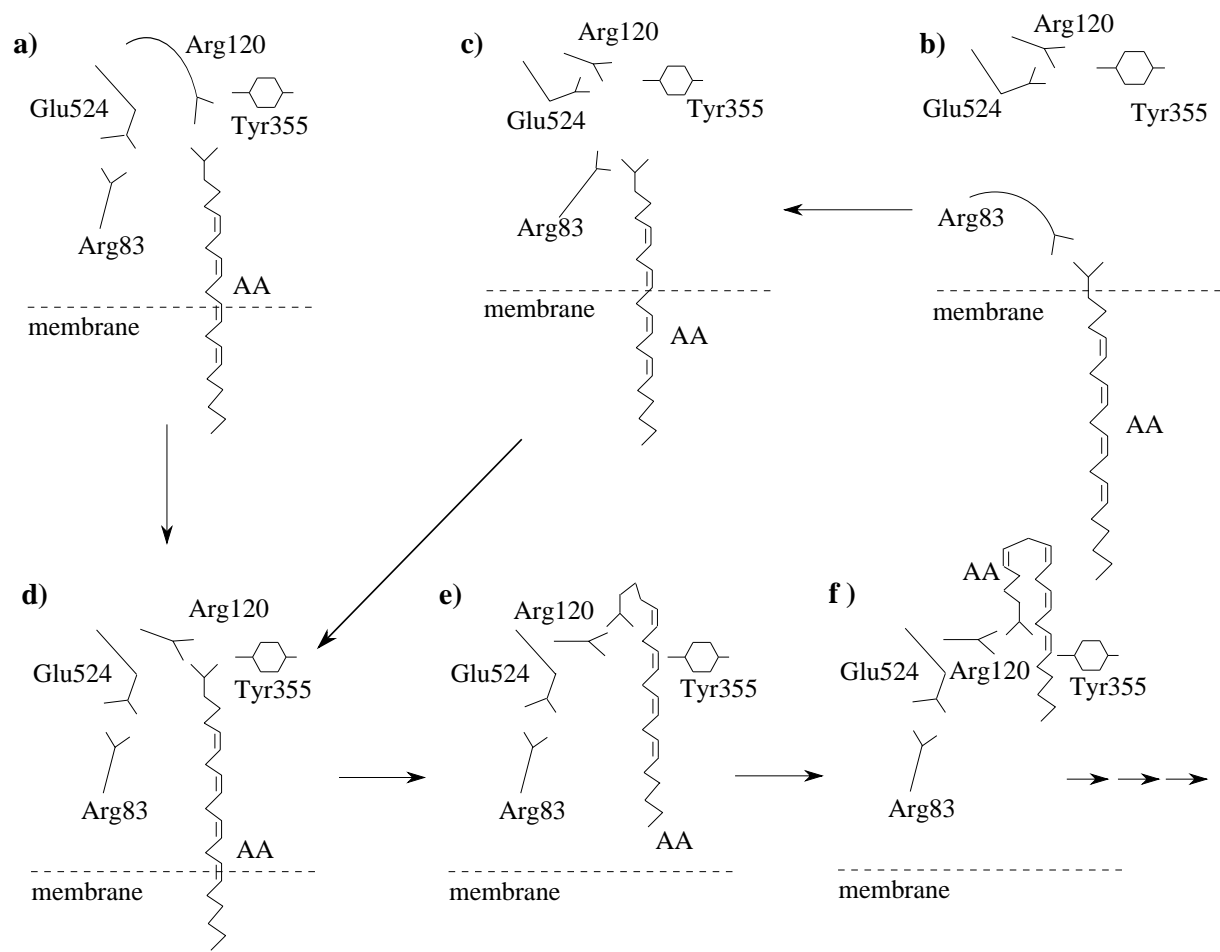


Figure 16: